

New Moons of Uranus and Neptune from Ultra-Deep Pencil Beam Surveys

SCOTT S. SHEPPARD,¹ DAVID J. THOLEN,² MARINA BROZOVIC,³ ROBERT JACOBSON,³
CHADWICK A. TRUJILLO,⁴ PATRYK SOFIA LYKAWKA,⁵ AND MIKE ALEXANDERSEN⁶

¹*Earth and Planets Laboratory, Carnegie Institution for Science, 5241 Broad Branch Rd. NW, Washington, DC 20015, USA, ssheppard@carnegiescience.edu*

²*Institute for Astronomy, University of Hawai'i, Honolulu, HI 96822, USA*

³*Jet Propulsion Laboratory, California Institute of Technology, 4800 Oak Grove Drive, Pasadena, CA 91109, USA*

⁴*Department of Astronomy and Planetary Science, Northern Arizona University, Flagstaff, AZ 86011, USA*

⁵*Kindai University, Shinkamikosaka 228-3, Higashiosaka, Osaka, 577-0813, Japan*

⁶*Center for Astrophysics | Harvard & Smithsonian, 60 Garden Street, Cambridge, MA 02138, USA*

ABSTRACT

We have conducted extremely ultra-deep pencil beam observations for new satellites around both Uranus and Neptune. Tens of images on several different nights in 2021, 2022 and 2023 were obtained and shifted and added together to reach as faint as 26.9 and 27.2 magnitudes in the r-band around Uranus and Neptune, respectively. One new moon of Uranus, S/2023 U1, and two new moons of Neptune, S/2021 N1 and S/2002 N5, were found. S/2023 U1 was 26.6 mags, is about 7 km in diameter and has a distant, eccentric and inclined retrograde orbit similar to Caliban and Stephano, implying these satellites are fragments from a once larger parent satellite. S/2021 N1 was 26.9 mags, about 14 km in size and has a retrograde orbit similar to Neso and Psamathe, indicating they are a dynamical family. We find S/2021 N1 is in a Kozai-Lidov orbital resonance. S/2002 N5 was 25.9 mags, is about 23 km in size and it makes a family of distant prograde satellites with Sao and Laomedea. This survey mostly completes the outer satellites of Uranus to about 8 km and Neptune to about 14 km in diameter. The size distributions of satellite dynamical families around the giant planets shows a strong steepening in the power law size distribution smaller than 5 km in diameter. The satellites of a family become much more common smaller than 5 km and their size distribution is consistent with a collisional break-up of a once larger parent satellite.

1. INTRODUCTION

The giant planets are known to have many satellites that can be classified as either small inner prograde satellites, medium to large regular prograde satellites or small outer irregular satellites. The regular satellites, like the four large Galilean satellites around Jupiter, are thought to have formed with the planet in a circumplanetary disk of gas and dust (Canup & Ward 2002; Cuk et al. 2020a; Batygin & Morbidelli 2020). The small inner satellites are close to the planet where collisions, tidal forces and the Roche radius limit of the planet creates a chaotic environment that can perturb and/or disrupt these satellites over the age of the solar system (Cuk et al. 2020b, 2022; Kane & Li 2023). Many of the small inner giant planet satellites are associated with rings of the giant planets (French et al. 2015; Charnoz et al. 2018). The regular satellites of the planets are generally medium to large satellites that can easily be observed with modern telescopes (Salmon & Canup 2017; Neveu

& Rhoden 2019). The inner small satellites are best discovered by spacecraft like Voyager 2 and Cassini or spaced-based observatories like the Hubble Space Telescope, which have small fields-of-view, but high resolving and deep imaging power to deal with the strong scattered light near a planet (Showalter et al. 2019).

The outer satellites have irregular, distant, inclined and eccentric orbits that can be either prograde or retrograde, which suggests they did not form with the planet, but were captured during or just after the planets formed (Jewitt & Haghighipour 2007; Nicholson et al. 2008; Nesvorny 2018). Current capture of a satellite by a planet is not efficient in the solar system, but in the past several mechanisms were operating more prominently that could remove energy from the orbit of a passing object to make satellite capture more probable. These capture mechanisms include close planet-planet encounters (Cuk & Gladman 2006; Nesvorny et al. 2007), gas drag (Cuk & Burns 2004), and collisions or three body interactions within the Hill Sphere of a planet of passing comets or asteroids (Colombo & Franklin 1971; Vokrouhlicky et al. 2008; Philpott et al. 2010; Koch & Hansen 2011; Gaspar et al. 2013).

The number and configuration of planetary outer satellites are interesting in the context of planet formation and migration (Jewitt & Sheppard 2005; Jewitt & Haghighipour 2007; Nicholson et al. 2008; Nesvorny 2018). Remarkably, all the giant planets appear to have similar outer satellite systems for the largest few satellites (> 20 km), even though these planets had different formation histories (Sheppard et al. 2006). This suggests the capture of these outer planetary satellites occurred just after the planet formation epoch, and their capture was independent of the planet's mass or formation location. The outer satellites could be windows into the planet building and migration process as they were likely captured during the Solar System's earliest days.

Jupiter currently has 95 known satellites of which 87 are outer irregular satellites, Saturn has 146 with 122 outer satellites, Uranus, with this work, now has 28 with 10 outer satellites and Neptune 16 with 8 outer satellites. Many of the outer satellites of Jupiter and Saturn have been shown or thought to be in dynamical orbital families, suggesting there were originally only a few outer parent satellites that had broken apart from collisions with asteroids, comets or other satellites over the age of the solar system. Jupiter appears to have 7 or 8 dynamically unique outer satellite type orbits (Sheppard & Jewitt 2003; Beauge & Nesvorny 2007; Brozovic & Jacobson 2017; Sheppard et al. 2018, 2023), while Saturn has 5 or more dynamically unique outer satellite type orbits (Gladman et al. 2001; Holt et al. 2018; Ashton et al. 2022; Jacobson et al. 2022; Sheppard et al. 2023). Until now, it was not clear if Uranus and Neptune had dynamical outer satellite families since only the largest have been found to date. It has been suggested the Uranian satellites Caliban and Stephano could be the largest members of a group, but having just two objects makes this suggestion indeterminate (Nesvorny et al. (2003); Kavelaars et al. (2004); Sheppard et al. (2005)). Neptune also has no obvious groupings of its largest outer satellites, though the retrogrades Neso and Psamathe have similar orbits suggesting a grouping as mentioned in Sheppard et al. (2005). The outer Neptune prograde satellites Sao and Laomedeia could also make a possible grouping (Holman et al. 2004). If these are true groups at Uranus and Neptune, it would be expected that many more smaller satellites should exist with similar orbits, like seen for Jupiter and Saturn.

Uranus and Neptune both have peculiarities that might have disrupted their satellite systems. Uranus is tipped on its side with a > 90 deg obliquity, likely from a giant impact during the planet formation process (Parisi et al. 2008; Rufu & Canup 2022). Uranus' outer satellites do appear

somewhat unique in that the retrograde satellites are closer to the planet and Uranus does not have a significant prograde outer satellite population (Figure 1). Neptune likely captured the large Kuiper Belt object Triton, which is bigger than Pluto. Triton, the largest retrograde satellite by far in the solar system (~ 2700 km), possesses a near circular and relatively close-in orbit to Neptune. Intriguingly, Nereid, the largest distant outer satellite of Neptune at about 360 km, has the most eccentric orbit of any known satellite, but interestingly a low inclination and relatively small semi-major axis. This suggests Nereid might have once been an inner satellite that formed with Neptune and was disrupted from Triton’s capture. In particular, the origin of Triton can unveil important constraints on the formation or survival of Nereid and the remaining smaller outer satellites (Agnor & Hamilton, 2006; Rufu & Canup 2017). Triton and/or Nereid could be captured objects from the Kuiper Belt or ejected former inner satellites (Nogueira et al. 2011; Li & Christou 2020; Gomes & Morbidelli 2024). The remaining outer satellites of Neptune were probably captured from heliocentric orbit as they have more traditional irregular outer satellite type orbits (Holman et al. 2004; Sheppard et al. 2006; Nesvorny et al. 2014; Li et al. 2020).

The size distribution of Uranus and Neptune satellites are poorly understood because only the brightest and thus largest are known. For this reason, models of collisional evolution of giant planets’ outer satellites do not usually considered Neptune while collisional models use an incomplete Uranus satellite system (Bottke et al. 2010). Shallow size distributions are seen for the outer satellites between 20 and 100 km for Jupiter, Saturn, Uranus and Neptune (Sheppard et al. 2006). There is a steepening in the distribution at sizes less than 15 km at Jupiter and Saturn (Sheppard & Jewitt 2003; Nicholson et al. 2008; Sheppard et al. 2018, 2023; Ashton et al. 2020, 2021). This is a sign of strong collisional evolution at Jupiter and Saturn as groups of these numerous smaller satellites tend to have dynamically similar orbits, showing a fragmentation of a once larger satellite (Figure 1). Bottke et al. (2010) required substantial depletion of captured outer satellites via collisional evolution to satisfy observations.

For the much more numerous small outer satellites of only a few km in size, it is unknown if Uranus and Neptune continue the trend of similar outer satellite systems as Jupiter and Saturn since it is very hard to discover small satellites at Uranus’ and Neptune’s extreme distances. Jupiter’s outer satellites are complete to about 2 km and Saturn to about 3 km because of their closer distance to Earth (Sheppard et al. 2023). To better compare Uranus’ and Neptune’s system to the other planets, we must search for satellites smaller than the power law size break that likely occurs below about 15 km in satellite size. Discovery of smaller outer satellites will help to better understand the collisional evolution in these systems and better compare them to the similar Trojan asteroids and Kuiper Belt (Bottke et al. 2023a). In addition, future spacecraft missions to Uranus or Neptune may be able to image some of the outer satellites of these planets (Denk & Mottola 2019; Cartwright et al. 2021; Cohen et al. 2022).

For the outer satellites of the giant planets, the sky area needed to search for stable satellites around a planet is so large, they can only efficiently be discovered by large field-of-view ground-based telescopes. The last successful ground-based surveys for satellites of Uranus and Neptune were done about two decades ago, reaching about 25.5 to 26th magnitude in the r-band and able to detect satellites larger than about 15 and 30 km around Uranus and Neptune, respectively (Kavelaars et al. 2004; Holman et al. 2004; Sheppard et al. 2005, 2006; Brozovic et al. 2011). We here report on a new survey of the region around Uranus and Neptune to extra ultra-deep depths using the Magellan

6.5m and Subaru 8.2m telescopes, going more than a magnitude fainter than previous observations to over 27th mags. This very ultra-deep survey was done by imaging the Hill spheres of Uranus and Neptune with tens of images over several hours on several different nights and then shifting and adding the images together at the planets' motion to detect faint satellites not normally visible in a single image.

2. OBSERVATIONS AND METHODS

We used the Subaru and Magellan telescopes to observe most of the dynamically stable Hill Spheres of Uranus and Neptune to extra ultra-faint depths through a pencil-beam survey. Subaru has a 8.2 meter primary mirror and uses the Hyper Suprime-Cam (HSC) imager at prime focus (Miyazaki et al. 2018; Komiyama et al. 2018; Kawanomoto et al. 2018; Furusawa et al 2018). HSC covers about a 1.5 degree diameter and has 112 individual CCDs that are 2048×4096 pixels. The pixel size is 0.168 arcseconds per pixel. The r-band filter was used. We also used the 6.5 meter Magellan telescope for discovery and recovery with the Inamori Magellan Areal Camera and Spectrograph (IMACS) camera at the F/2 focus, which has 8 CCDs of 2048×4096 pixels and a pixel scale of 0.20 arcseconds per pixel (Dressler et al. 2011). The very wide band filter WB4800-7800 was used, which covers a wavelength range from 4800 to 7800 angstroms that is similar to a very broad VR filter. The IMACS field-of-view is about 0.17 square degrees.

Neptune's and Uranus' Hill Spheres, where satellites are theoretically stable, are about 1.5 degs (0.78 au) and 1.4 degs (0.49 au) in radius on the sky, respectively. But simulations, analytical analysis and empirical data from other planets show that outer satellites are only stable to about 0.7 Hill radii for retrograde and 0.5 Hill radii for prograde satellites, making the true area that satellites are stable at about 1 degree radius or less on the sky (Hamilton & Krivov 1997; Sheppard et al. 2006; Shen & Tremaine 2008; Donnison 2011). In addition, projection effects of a satellite orbit onto the sky makes even the largest satellite orbits usually appear well less than 0.7 Hill radii away from the planet on sky, even when the satellites are near the extremes of their orbits. HSC covers most of the stable Uranus or Neptune Hill Spheres in one image when the planet is placed near the center of the field, but IMACS does not and thus requires multiple pointings to cover the primary inner Hill Sphere of a giant planet.

The extra ultra-faint magnitudes we need to achieve are not possible in a single exposure due to the background saturation of the CCDs that would occur after several minutes of exposing. The satellites also move relative to the background stars and galaxies, making the satellites trail after just a few minutes of exposure when guiding the telescope at sidereal rates. Because of the background saturation problem in very long exposures and the movement of the satellites at non-sidereal rates, we used a shifting and adding/medianing of the images taken during a single night to get to extra ultra-faint magnitudes that we required to explore the smaller sized satellite populations around these planets. The Image Reduction and Analysis Facility (IRAF) with the imshift and imcombine routines was used on images from a given night to shift them by the apparent motion of the respective planet and then add them together to get one single extra ultra-deep image. The same images were also shifted and medianed together to get a second type of extra ultra-deep image. In such a deep image the stars and galaxies appear trailed, while any object with a motion similar to the planet will be seen as a point source, making very faint satellites discernible from the background noise. Using this time intensive technique on some of the largest telescopes in the world allowed the images to reach fainter magnitudes around Uranus and Neptune than any previous observations.

Satellites were searched for in three complementary ways in all of the data taken. First, the co-added images were examined by eye for any point sources. Second, the median images were examined by eye for any point sources. The co-added and medianed images were then compared at the location of any detected point sources to determine if the source was likely to be real or just a hot pixel or cosmic ray, which appear more prominent in the the co-added images compared to the medianed images. Finally, the first half and second half of each night’s data were co-added as well as medianed together and then visually compared to look for moving objects, which the eye can identify at Signal-to-Noise levels of about 3.5. All these techniques have similar depths of identifying real objects, with the medianed images usually giving slightly better results. We used the known Neptune and Uranus satellites found in the data along with implanting fake objects into the data to determine our limiting magnitude for each observation. As done in previous moving object surveys, we used the `imexam` routine in IRAF to determine the point-spread function of each image to generate artificial objects with the IRAF routine `mkobjects` that were implanted into the images (Sheppard and Trujillo 2016). Figure 2 shows the typical efficiency curve of finding moving objects in a median single night dataset, which gives us our limiting magnitudes for each nights data shown in Table 1.

With deep recovery imaging of newly found satellites, we duplicated large areas of coverage around both Uranus and Neptune in three different years, 2021, 2022 and 2023 at multiple different times during a single year. This means satellites that may have been originally obscured by a background star or out of the field-of-view in one month or year would likely not be so in a following time, making the survey more complete. This completeness is demonstrated by our recovery multiple times of all known outer satellites of both Uranus and Neptune, without prior knowledge of their locations.

2.1. *Neptune Satellite Pencil Beam Survey*

Subaru HSC was used on the nights of UT September 7 and 8, 2021 with Neptune placed near the center of the field-of-view. Nineteen images of 350 seconds were taken on September 7 and twelve images on September 8 (Figure 3). The average seeing for the Neptune images on September 7th was 0.83 arcseconds and 0.77 arcseconds on September 8th (see Table 1). S/2021 N1 was found on both nights of the Subaru Neptune observations (Sheppard et al. 2024a), as was S/2002 N5 on both nights, which was already found using Magellan a few days prior (Sheppard et al. 2024b).

We used Magellan to image to the West and East sides of Neptune on UT 3 September 2021, putting Neptune just outside the field-of-view for both long stares. The West imaging obtained sixteen images of 380 seconds in 0.73 arcsecond seeing and the East imaging had twenty-one images in 0.67 arcsecond seeing (Table 1). S/2002 N5 was found in the Neptune West images after co-adding them (Sheppard et al. 2024b).

After the main discovery images around Neptune from Subaru and Magellan in September 2021, we used Magellan again in October and December 2021 to recover the newly found Neptune satellites (Table 1). During the recoveries, we again searched the complete IMACS field-of-view for any possible missed satellites during the discovery images in September 2021, with nothing new found. The two new Neptune satellites were again imaged in 2022, the brighter S/2002 N5 at Magellan and the fainter S/2021 N1 at the VLT using the FORS2 imager. Gemini with the Gemini Multi-Object Spectrograph (GMOS) imager was used on UT 3 November 2023 to confirm the faintest of the new Neptune satellites (Hook et al. 2004). Both new Neptune satellites were imaged at Magellan on UT 4 November 2023 to fully determine their orbits and they were announced on Minor Planet Electronic

Circulars in February 2024 (Sheppard et al. 2024a, 2024b). All recovery images were fully searched to look for additional new satellites, with no new satellites found.

As shown in Figure 2 the Neptune Subaru survey on September 7 had a limiting magnitude of 27.2 mags while the September 8 observations, which repeated the same area of space around Neptune, had a limiting magnitude of 26.9 mags. In addition, several Magellan ultra-deep images were taken near Neptune with depths as faint as 26.9 mags (see Table 1). All known Neptune outer satellites were detected on multiple nights in these observations and astrometry reported to the Minor Planet Center shown in Table 2 as many had not been observed for several years, some not since 2009. From these observations, the outer satellites of Neptune should be nearly complete to about 27 mags, corresponding to satellites of about 14 km in diameter assuming albedos of 0.1.

2.2. *Uranus Satellite Pencil Beam Survey*

Uranus was placed near the center of the field-of-view using Subaru on 8 September 2021 with twelve images of 300 seconds taken in average seeing of 0.73 arcseconds (see Table 1 for details). The Uranus images using Subaru were not as deep as those for Neptune since only twelve images of 300 seconds were taken on only one night for Uranus, while Neptune had nineteen images of 350 seconds on one night and another twelve on a second night. In addition, Uranus was off-opposition in September, which amounted to losing about 0.3 magnitudes in brightness for the satellites from the increased distance from Earth and the higher phase angle. In the co-added and medianed images, a very faint object was identified as a point source and moving at Uranus' rate, but was too faint to be a reliable detection to use significant large telescope time to follow-up. A few brighter candidates that were moving a little off of Uranus' motion were imaged at Gemini a month later and found to not be Uranus satellites.

Fields around Uranus were further imaged using Magellan to extra ultra-faint depths in late October and early December 2021, allowing all four quadrants around Uranus to be again deeply imaged using Magellan (Figure 4). The Magellan imaging cycle for one field lasted 2 to 4 hours on each night (Table 1). No obvious new satellites of Uranus were detected in the 2021 images, though a faint almost in the noise source was flagged in the Magellan images, but it was near a bright star and deemed too faint and questionable as a source to use a significant amount of large telescope time to follow-up. Since there might be very faint unconfirmed satellites around Uranus, the main space around Uranus was again imaged for new satellites at Magellan on 4 November 2023 with Uranus placed at the center of the field-of-view (Figure 5). One new candidate Uranus satellite was detected and follow-up imaging at Magellan on December 6 and 13 showed this source as likely being a new Uranian satellite. A basic Uranian satellite orbit was determined for the newly found object based on the 3 observations in late 2023, which was able to link the very faint sources noticed at both Subaru and Magellan in the 2021 data to the 2023 observations. With over two years of observations, S/2023 U1 was announced on a Minor Planet Electronic Circular in February 2024 (Sheppard et al. 2024c).

All known Uranus outer satellites were easily detected in our survey images on at least two different observing nights without prior knowledge of their locations. The new astrometry shown in Table 3 was reported to the Minor Planet Center as some of these known satellites had not been observed since 2004. We covered the inner 77 percent of Uranus' stable Hill sphere radius to depths of 26.5 to 26.9 mags. The very inner region around Uranus where most satellites would expect to be found was observed with overlapping fields in 2021 as well as having our deepest Magellan image centered

on Uranus in 2023 to 26.9 mags. The outer satellites of Uranus should be nearly complete to about 26.5 mags, corresponding to satellites of about 8 km in diameter assuming albedos of 0.1.

3. RESULTS

We found three new satellites, one around Uranus and two around Neptune. The new Uranus and Neptune satellites are the faintest ever discovered around the planets using ground-based telescopes. In addition, we also detected all known outer satellites of Uranus and Neptune on multiple nights, some not seen since 2004.

All of the new Uranian and Neptunian satellites have distant, eccentric and inclined orbits that suggests they were captured satellites, which likely occurred during or just after the planet formation epoch (Figure 1). These new observations around the outer planets nearly complete the satellite inventories of Uranus and Neptune to about 26.5 and 27 mags or about 8 and 14 km, respectively, assuming albedos of the satellites of ten percent (see Table 1). Jupiter is complete to about 2 km in size, while Saturn is complete to about 3 km in size for satellites, with the closer planets better positioned to find fainter and thus smaller satellites (Sheppard et al. 2023).

3.1. *New Uranian Satellite S/2023 U1*

The newly discovered Uranus satellite is provisionally named S/2023 U1, and this now gives Uranus 28 known satellites, of which 10 are outer irregular satellites. The new Uranian satellite has over 2 years of observations and thus a secure well-determined orbit around Uranus (Table 4). S/2023 U1 is about 7 km in diameter assuming an albedo of ten percent, likely making it the smallest satellite ever observed around Uranus. It has a distant and inclined retrograde orbit around Uranus, taking about 1.86 years to orbit Uranus once. This orbit is similar to Uranian outer satellites Caliban and Stephano. S/2023 U1 will receive a permanent number and name based on a Shakespeare character.

3.2. *New Neptunian Satellites S/2021 N1 and S/2002 N5*

Two new satellites of Neptune were discovered. Neptune now has 16 known satellites, of which 8 are outer irregular satellites plus Triton. The fainter Neptune satellite has a provisional designation S/2021 N1 and is the faintest satellite ever discovered at 26.9 mags by ground-based observations. S/2021 N1 is about 14 km in diameter with a distant retrograde orbit around Neptune of almost 27 years (Table 4). S/2021 N1 has an orbit that is similar to Neptunian outer satellites Neso and Psamathe.

Once an orbit around Neptune was determined for the brighter new Neptune satellite using the 2021, 2022 and 2023 observations, it was traced back to an object that was spotted near Neptune in 2002, but lost before it could be confirmed as orbiting Neptune (Holman et al. 2004). The brighter Neptune satellite now has a provisional designation S/2002 N5 with a prograde orbit of almost 9 years to orbit Neptune and is about 23 km in diameter (Table 4). S/2002 N5 has an orbit that is similar to Neptunian outer satellites Sao and Laomedea. The new Neptune satellites have over two years of observations and thus secure well determined orbits and will get permanent numbers and names based on the fifty Nereid sea goddesses in Greek mythology.

3.3. *Keplerian Osculating Orbital Elements of Outer Satellites*

The outer satellites of the giant planets have significant gravitational interactions with the other giant planets as well as the Sun. Thus the orbits of the satellites are not closed orbits but may vary

over time. Using the new 2021, 2022 and 2023 astrometry obtained on all of the outer satellites of Uranus and Neptune, we performed numerical integrations to determine the average, minimum and maximum variations (osculating elements) in the orbits of the known outer satellites over 10,000 years. Results are the Neptune satellite orbits nep104 and Uranus satellite orbits ura117 in the JPL *Horizons* On-Line Solar System Data Service (Giorgini et al. 1996) and from NASA's Navigation and Ancillary Information Facility (Acton 1996) (ssd.jpl.nasa.gov/sats/ephem/files.html). For the numerical simulations, we use the same parameters and techniques as detailed in Brozovic & Jacobson (2022). This dynamical model was also previously used for numerically integrated ephemerides of the outer irregular satellites in Jacobson et al. (2012), Brozovic & Jacobson (2017) and Jacobson et al. (2022). In brief, we add the masses of Mercury, Venus, the Earth-Moon system and Mars as part of the Sun's mass. For Uranus additional perturbers used are the planet Uranus, Uranus J2, Uranus J4 and its largest satellites Miranda, Umbriel, Ariel, Oberon and Titania along with the Jovian system, Saturnian system, and Neptunian system. For Neptune additional perturbers used are the planet Neptune, Neptune J2, Neptune J4, Neptune J6 and its largest satellite Triton as well as the Jovian system, Saturnian system and Uranian system (see Brozovic & Jacobson (2022) for full information). The JPL planetary ephemeris DE441 is used to determine the location of the planets and Sun and simulate the long-term dynamics of the satellites (Park et al. 2021).

The elemental space of all of the outer satellites of Uranus and Neptune based on their osculating orbits can be seen in Figures 6 and 7. A dynamical grouping of satellites suggesting a common origin from a once bigger parent body is likely if both the semi-major axis and inclination overlap for two or more objects in their osculating orbital elements over time. Tables 5 and 6 show mean osculating elements for 10,000 years of orbit integration.

The osculating orbital elements show there are dynamical orbital groupings of outer satellites around both Uranus and Neptune, like seen at Jupiter and Saturn. We find each of the newly discovered satellites reported here are likely in a dynamical grouping (see below), which show for the first time Uranian and Neptunian dynamical groups containing each three members. This suggests once larger parents satellites at Uranus and Neptune had broken apart due to past collisions, most likely with other moons, comets or asteroids, leaving the broken fragments behind in similar orbits as the original larger satellite. If these are really collisional remnants of once larger satellites, it is likely many smaller satellites exist in these newly identified Uranian and Neptunian groupings, like found at Jupiter and Saturn, but they would be only a few km in size or smaller and too faint to efficiently detect with current telescope and detector technology.

3.4. *Dispersion Velocities of Satellite Dynamical Groupings*

Another way to determine dynamical groupings of objects is to examine their dispersion velocities of their orbits relative to each other. The initial dispersion velocity would be expected to be near the escape speed of a disrupted body (Durda 2007). Most asteroid families would be expected to have initial dispersion velocities less than 100 m/s (Michel et al. 2015; Nesvorný et al. 2015). These initial dispersion velocities would likely grow in time through various perturbations over time (Carruba & Nesvorný 2016; Li & Christou 2018).

Collisional disruption of a small satellite around a planet is less well understood than that for asteroids in heliocentric orbit (Nesvorný et al. 2003; Bottke et al. 2024b). Not only are the physical characteristics of the satellites poorly understood, but a satellite around a planet may experience significantly different forces that could increase the dispersion velocity between family members

(Nesvorny et al. 2004). Outer satellites of the planets experience significant three-body interactions involving the Sun or other planets as well as various resonances such as the Kozai-Lidov resonance that we find to be operating on some, but not all, members of a dynamical family (Carruba et al. 2002, 2004; Beauge & Nesvorny 2007; Frouard et al. 2011; Brozovic and Jacobson 2022).

The prograde Himalia family of outer satellites at Jupiter has a very high dispersion velocity of up to 400 m/s (Li & Christou 2017), while the retrograde groups Carme and Ananke at Jupiter have about 50 and 80 m/s (Nesvorny et al. 2004). We assume any two objects with a minimum dispersion velocity of less than about 100 m/s have a good chance of being fragments from the same parent body.

We conducted a velocity dispersion simulation for the new Uranian and Neptunian dynamical groupings. The following metric for distance between elements of two different satellite was used (Beauge & Nesvorny 2007):

$$d_4^2 = C_a \left(\frac{\Delta a}{a} \right)^2 + C_e (\Delta e)^2 + C_I (\Delta \sin(I))^2 \quad (1)$$

Where Δa is difference in osculating semi-major axis between two satellites, Δe is for eccentricity, and $\Delta \sin(I)$ is for sinus of inclination. In addition, $C_a = \frac{(1-\bar{e}^2)^2}{4\bar{e}^2}$, $C_e = 1/2$, and $C_I = 2$.

The dispersion velocity for the group is defined as:

$$(\delta V)^2 = \frac{\mu}{\bar{a}(1-\bar{e}^2)} d_4^2 \quad (2)$$

where $\mu = GM_p$, G is the gravitational constant, M_p is the mass of the planet, \bar{e} and \bar{a} are the averaged eccentricity and averaged semi-major axis of all group members. We used 30,000 years of osculating elements and calculated the dispersion velocity every 100 days. Table 7 shows the results of the dispersion velocity simulations of all likely members. It is clear the three newest discoveries all have the lowest dispersion velocities among group members, indicating that these smaller satellites are probably collisional fragments of once larger satellites.

3.5. Uranian Caliban Dynamical Group

At Uranus, S/2023 U1 has a similar orbit as Caliban and Stephano (Table 5), making this a group of three satellites that is labeled as the Caliban group in Figure 1. In fact, S/2023 U1 has such a similar orbit as Stephano they almost completely overlap the phase space of each other (Figure 8). Their minimum dispersion velocity is only 21 m/s (Table 7). We find these objects come within about 22,000 km of each other in a few thousand years. This is strong evidence that S/2023 U1 and Stephano originated from the same parent body. Caliban, the other possible group member, overlaps with S/2023 U1 and Stephano in inclination, but has a slightly smaller semi-major axis that does not quite overlap with the osculating orbital elements of Stephano and S/2023 U1. This might suggest the smaller satellite S/2023 U1 was created from an impact into Stephano after the original event that created Caliban and Stephano. The Caliban family with S/2023 U1 shows that the outer irregular satellites of Uranus likely have broken apart and it is possible the dust produced from these events may create the red material seen on the leading hemispheres of some of the inner large Uranian satellites Titania, Oberon and Umbriel (Tamayo et al. 2013; Cartwright et al. 2018, 2023; Graykowski & Jewitt 2018).

Caliban has recently been observed in the infrared with a tentative detection in the thermal from Herschel observations, measuring a possible diameter of 42_{-12}^{+20} km (Farkas-Takacs et al. 2017; Sharkey et al. 2023). Stephano is about half the size of Caliban and S/2023 U1 much smaller at about 7 km in diameter. This would make the effective diameter of the parent satellite that may have created this dynamical group about 45 km in diameter, with Caliban having about 90% of the total volume of the three known members.

3.6. *Neptunian Neso Dynamical Group*

At Neptune, S/2021 N1 has a similar retrograde orbit as Psamathe and Neso called the Neso group in Figure 1. We find S/2021 N1 is in a Kozai-Lidov resonance, like Neso (Figure 9). The other member of the Neso Neptunian satellite group, Psamathe, does not appear to be in the Kozai-Lidov resonance (Figure 10). The Neso dynamical group is a strong dynamical grouping as both the semi-major axis and inclination osculating orbital elements overlap for all three objects and they have minimum dispersion velocities all below 100 m/s (Tables 6 and 7). Neso has about 80% of the total volume of the group and the parent satellite of the Neso group would have had a diameter of about 44 km assuming an albedo of 0.1.

3.7. *Neptunian Sao Dynamical Group*

S/2002 N5 has a similar prograde orbit to Sao and Laomedeia that is labeled the Sao group in Figure 1. The new satellite S/2002 N5 currently has a semi-major axis and inclination between the two brighter, and presumably larger satellites Sao and Laomedeia. The Sao group’s members all overlap in semi-major axis and inclination osculating orbital elements (Table 6). They do have somewhat higher dispersion velocities than the other dynamical group at Neptune (Table 7), but most are still below a velocity dispersion minimum of 100 m/s and small enough that each object likely originated from the same parent body, especially with the Kozai-Lidov resonance effecting some of the satellites. Sao is in the Kozai-Lidov resonance (Holman et al. 2004), but is the only member of the Sao group to be in the Kozai-Lidov resonance (Figure 11).

The Sao group is unusual in that both the two largest members are of similar brightness and likely size with newly discovered S/2002 N5 just a few tenths of a magnitude fainter and thus likely just a few km smaller. The parent satellite of this group would have had an effective diameter of about 38 km assuming an albedo of 0.1.

4. SMALL OUTER SATELLITE SIZE DISTRIBUTIONS

In Figure 12 we plot the cumulative size distribution of the outer satellite dynamical families of the giant planets that have tight orbital clustering and more than two known members. Thus we do not use the Jupiter prograde Carpo group, which is unusual in that it only has two small members and no large member. We also do not use the Jupiter Pasiphae/Sinope group as it is not as tightly confined in orbital space as the other Jupiter satellite dynamical families, though it appears to have a similar size power law as the other Jupiter families with one or two large members and many more smaller members. We further do not use the Saturn Gallic group as it is not as tightly clustered as the Saturn Kiviuq and Siarnaq groups. The Gallic group, if a true dynamical family, would be unusual in that not only is it somewhat dispersed, but it has several large or medium sized members and very few small members known (Sheppard et al. 2023). It is unclear if there are Saturn retrograde dynamical families or not, so we do not use any of these Saturn retrograde satellites in our dynamical family size power law analysis.

It is seen in Figure 12 that there is generally a shallow size power law for the largest few satellites of a dynamical family and then a steep power law for the smaller satellites of a family, meaning many more small members (Sheppard & Jewitt 2003; Sheppard et al. 2006, 2018, 2023; Bottke et al. 2010; Alexandersen et al. 2012; Nesvorny 2018; Ashton et al. 2020, 2021). The cumulative number power-law size index is typically represented by q , where $N(> r) \propto r^q$. The standard Dohnanyi et al. (1972) collisional cumulative power law size frequency distribution index has a steep slope of $q \sim -2.5$, which we plot as a dotted line in Figure 12. We note that this steep slope, consistent with a collisional size distribution, starts for the smallest outer satellites around 5 km in diameter. This is consistent with an interpretation that most satellites smaller than 5 km are products of collisional disruption.

There is a significant increase in the number of satellites for a family starting around a diameter of 5 km. At Uranus and Neptune we have not yet efficiently surveyed for such small outer satellites, as mentioned above being only complete to about 8 and 14 km for outer satellites around these planets, respectively. Thus if the dynamical groups are from a once larger parent satellite, many more smaller and likely fainter satellites are expected to exist for the Caliban, Sao and Neso dynamical groups at Uranus and Neptune.

Besides the large satellites Triton and Nereid, which have much closer orbits to Neptune and may have been inner satellites as described in the introduction, the only other known normal outer irregular Neptune satellite is Halimede. Interestingly, Halimede, to date a lone member, is of a similar diameter as the parent satellites of the Neso and Sao Neptune dynamical Groups, being about 42 km in size assuming an albedo of 0.1. Thus Neptune might of only had three original distant outer irregular satellites, all of similar size: the Neso parent body, the Sao parent body and Halimede. One might expect there to be several lone or parent outer irregular satellites of Neptune in the 20 km size range, as smaller objects should have been more numerous and thus more likely to be captured as satellites. The lack of original ~ 20 km sized Neptune outer satellites might be a sign that asteroids formed big and were captured as satellites before significant break-up occurred to the asteroids (Morbidelli et al. 2009; Sheppard et al. 2010; Shankman et al. 2013; Johansen & Lambrechts 2017). If true, satellites at Neptune smaller than 40 to 50 km would likely only be found as fragments of larger parent objects, like appears to be the case for S/2021 N1 and S/2002 N5.

5. CONCLUSIONS AND SUMMARY

Through an extra ultra-deep pencil-beam survey of the space near Uranus and Neptune we have imaged over a magnitude fainter than previous surveys and found three new outer satellites. S/2023 U1 is a new retrograde Uranian satellite of 26.6 mags in the r-band, corresponding to about 7 km in diameter assuming a ten percent albedo. S/2021 N1 is a new retrograde Neptunian satellite that is 26.9 mags, corresponding to 14 km in diameter while S/2002 N5 is a prograde satellite and is 25.9 mags corresponding to 23 km in diameter. We detected, on multiple nights, all known outer satellites of Uranus and Neptune during these observations in 2021, 2022 and 2023. All new astrometry has been reported to the Minor Planet Center as some of these satellites have not been observed since 2004. These observations nearly complete the outer satellite populations of Uranus and Neptune to about 26.5 and 27 mags, corresponding to diameters of about 8 and 14 km assuming albedos of 0.1, respectively.

All the new satellite discoveries have osculating orbital elements that overlap significantly with two larger known satellites, as well as have low dispersion velocities with those same known satellites.

This gives three members for each of these identified dynamical families for the first time. At Uranus there is the retrograde Caliban group with Caliban, Stephano and S/2023 U1 where Stephano and S/2023 U1 overlap almost completely in osculating orbital phase space with a minimum dispersion velocity of only 21 m/s. The likely parent satellite of the Caliban group was about 45 km in diameter. This Uranian dynamical grouping shows outer irregular satellites of Uranus were likely broken apart over time and it is possible the dust produced from these events could be the source of the red material seen on the leading hemispheres of some the inner larger Uranian satellites.

At Neptune there is the prograde Sao dynamical group with Sao, Laomedea and S/2002 N5, where all three members overlap in osculating orbital phase space and have minimum dispersion velocities of less than 80 m/s with each other. The Sao group parent satellite may have had a diameter of about 38 km. The Neptune retrograde Neso group includes Neso, Psamathe and S/2021 N1, with the parent satellite about 44 km in diameter. We find that newly discovered S/2021 N1 is in a Kozai-Lidov resonance as its argument of pericenter librates around 90 degrees.

The satellite dynamical families of the giant planets significantly increase in the number of members for diameters less than about 5 km in diameter. Steep size distribution slopes consistent with collisional breakup of once larger parent satellites is seen for diameters less than 5 km. For both the Uranus and Neptune dynamical groups, we expect many more smaller satellites exist, but current surveys have not gone deep enough to efficiently discover satellites around these planets as small or smaller than 5 km in diameter. If most asteroids formed bigger than $\sim 40 - 50$ km in size through pebble accretion, this might explain the lack of ~ 20 km sized parent outer satellites at Neptune. Captured outer satellites at Neptune smaller than $\sim 40 - 50$ km may only be found as fragments of larger parent objects, like appears to be the case for S/2021 N1 and S/2002 N5.

ACKNOWLEDGMENTS

This paper includes data gathered with the 6.5 meter Magellan Telescopes located at Las Campanas Observatory, Chile. This research is based in part on data collected at the Subaru Telescope, which is operated by the National Astronomical Observatory of Japan. We are honored and grateful for the opportunity of observing the Universe from Maunakea, which has the cultural, historical, and natural significance in Hawaii. Based on observations obtained at the international Gemini Observatory, a program of NSF's NOIRLab, which is managed by the Association of Universities for Research in Astronomy (AURA) under a cooperative agreement with the National Science Foundation on behalf of the Gemini Observatory partnership: the National Science Foundation (United States), National Research Council (Canada), Agencia Nacional de Investigación y Desarrollo (Chile), Ministerio de Ciencia, Tecnología e Innovación (Argentina), Ministério da Ciência, Tecnologia, Inovações e Comunicações (Brazil), and Korea Astronomy and Space Science Institute (Republic of Korea). Gemini program ID GN-2023B-DD-102. Part of the research described here was carried out at the Jet Propulsion Laboratory, California Institute of Technology, under contract with the National Aeronautics and Space Administration (80NM0018D0004). Based on observations collected at the European Southern Observatory under ESO programme 110.259D.001.

REFERENCES

- Acton, C. 1996, P&SS, 44, 65.
- Agnor, C. & Hamilton, D. 2006, *Nature*, 441, 192.
- Alexandersen, M., Gladman, B., Veillet, C., Jacobson, R., Brozovic, M. & Rousselot, P. 2012, *AJ*, 144, 21.
- Ashton, E., Beaudoin, M. & Gladman, B. 2020, *PSJ*, 1, 52.
- Ashton, E., Gladman, B. & Beaudoin, M. 2021, *PSJ*, 2, 158.
- Ashton, E., Gladman, B., Beaudoin, M., Alexandersen, M. & Petit, J. 2022, *PSJ*, 3, 107.
- Batygin, K. & Morbidelli, A. 2020, *ApJ*, 894, 143.
- Beauge, C. & Nesvorný, D. 2007, *AJ*, 133, 2537.
- Bottke, W., Nesvorný, D., Vokrouhlický, D. & Morbidelli, A. 2010, *AJ*, 139, 994.
- Bottke, W., Marschall, R., Nesvorný, D. & Vokrouhlický, D. 2023, *SSR*, 219, 83.
- Bottke, W., Vokrouhlický, D., Marschall, R., Nesvorný, D., Morbidelli, A., Deienno, R., Marchi, S., Dones, L. & Levison, H. 2023, *PSJ*, 4, 168.
- Brozovic, M., Jacobson, R. & Sheppard, S. 2011, *AJ*, 141, 135.
- Brozovic, M. & Jacobson, R. 2017, *AJ*, 153, 147.
- Brozovic, M. & Jacobson, R. 2022, *AJ*, 163, 241.
- Canup, R. & Ward, W. 2002, *AJ*, 124, 3404.
- Carruba, V., Burns, J., Nicholson, P. & Gladman, B. 2002, *Icarus*, 158, 434.
- Carruba, V., Nesvorný, D., Burns, J., Cuk, M. & Tsiganis, K. 2004, *AJ*, 128, 1899.
- Carruba, V. & Nesvorný, D. 2016, *MNRAS*, 457, 1332.
- Charnoz, S., Canup, R., Crida, A. & Dones, L. 2018. *The Origin of Planetary Ring Systems. Planetary Ring Systems. Properties, Structure, and Evolution*, Matthew S. Tiscareno and Carl D. Murray (eds.) ISBN: 9781316286791, 2018., Cambridge University Press, p.517-538.
- Cartwright, R., Emery, J., Pinilla-Alonso, N., Lucas, M., Rivkin, A. & Trilling, D. 2018, *Icarus*, 314, 210.
- Cartwright, R., Beddingfield, C., Nordheim, T. et al. 2021, *PSJ*, 2, 120.
- Cartwright, R., DeColibus, R., Castillo-Rogez, J., Beddingfield, C., Grundy, W. & Nordheim, T. 2023, *PSJ*, 4, 42.
- Colombo, G. & Franklin, F. 1971, *Icarus*, 15, 186.
- Cohen, I., Beddingfield, C., Chancia, R. et al. 2022, *PSJ*, 3, 58.
- Cuk, M. & Burns, J. 2004, *Icarus*, 167, 369.
- Cuk, M. & Gladman, B. 2006, *Icarus*, 183, 362.
- Cuk, M., El Moutamid, M. & Tiscareno, M. 2020a, *PSJ*, 1, 22.
- Cuk, M., French, R., Showalter, M., Tiscareno, M. & El Moutamid, M. 2022, *AJ*, 164, 38.
- Denk, T. & Mottola, S. 2019, *Icarus*, 322, 80.
- Dohnanyi, J. 1972, *Icarus*, 17, 1.
- Donnison, J. 2011, *MNRAS*, 415, 470.
- Dressler, A., Bigelow, B., Hare, T., et al. 2011, *PASP*, 123, 288.
- Durda, D., Bottke, W., Nesvorný, D., Enke, B., Merline, W., Asphaug, E. & Richardson, D. 2007, *Icarus*, 186, 498.
- Farkas-Takacs, A., Kiss, C., Pal, A. et al. 2017, *AJ*, 154, 119.
- French, R., Dawson, R. & Showalter, M. 2015, *AJ*, 149, 142.
- Frouard, J., Vienne, A. & Fouchard, M. *A&A*, 2011, 532, 44.
- Furusawa, H. et al. 2018, *PASJ*, 70, S3.
- Gaspar, H., Winter, O. & Vieira Neto, E. 2013, *MNRAS*, 433, 36.
- Giorgini, J., Yeomans, D., Chamberlin, A. et al. 1996, *AAS/DPS Meeting Abstracts*, 28, 25.04.
- Gladman, B., Kavelaars, J., Holman, M., et al. 2001, *Nature*, 412, 163.
- Gomes, R. & Morbidelli, A. 2024, *Icarus*, 420, 116142.
- Graykowski, A. & Jewitt, D. 2018, *AJ*, 155, 184.
- Hamilton, D. & Krivov, A. 1997, *Icarus*, 128, 241.
- Holman, M., Kavelaars, J., Grav, T. et al. 2004, *Nature*, 430, 865.
- Holt, T., Brown, A., Nesvorný, D., Horner, J., & Carter, B. 2018, *ApJ*, 859, 97.
- Hook, I., Jorgensen, I., Allington-Smith, J., Davies, R., Metcalfe, N., Murowinski, R. & Crampton, D. 2004, *PASP*, 116, 425.
- Jacobson, R., Brozovic, M., Gladman, B., Alexandersen, M., Nicholson, P. & Veillet, C. 2012, *AJ*, 144, 132.
- Jacobson, R., Brozovic, M., Mastrodemos, N., Riedel, J. & Sheppard, S. 2022, *AJ*, 164, 240.
- Jewitt, D. & Sheppard, S. 2005, *SSR*, 116, 441.
- Jewitt, D. & Haghighipour, N. 2007, *ARAA*, 45, 261.
- Johansen, A. & Lambrechts, M. 2017, *AREPS*, 45, 359.
- Kane, S. & Li, Z. 2023, *PSJ*, 4, 216.
- Kavelaars, J., Holman, M., Grav, T., Millisavljevic, D., Fraser, W., Gladman, B., Petit, J., Rousselot, P., Mousis, O. & Nicholson, P. 2004, *Icarus*, 169, 474.
- Kawanomoto, S. et al. 2018, *PASJ*, 70, 66.
- Koch, E. & Hansen, B. 2011, *MNRAS*, 416, 1274.
- Komiyama, Y. et al. 2018, *PASJ*, 70, S2.
- Li, D. & Christou, A. 2017, *AJ*, 154, 209.
- Li, D. & Christou, A. 2018, *Icarus*, 310, 77.
- Li, D. & Christou, A. 2020, *AJ*, 159, 184.
- Li, D., Johansen, A., Mustill, A., Davies, M. & Christou, A. 2020, *AA*, 638, A139.
- Michel, P., Richardson, D., Durda, D., Jutzi, M., Asphaug, E., 2015. *Collisional Formation and Modeling of Asteroid Families. Asteroids IV*, Patrick Michel, Francesca E. DeMeo, and William F. Bottke (eds.), University of Arizona Press, Tucson, 895 pp. ISBN: 978-0-816-53213-1, 2015., p.341-354.
- Miyazaki, S. et al. 2018, *PASJ*, 70, S1.
- Morbidelli, A., Bottke, W., Nesvorný, D. & Levison, H. 2009, *Icarus*, 204, 558.
- Nesvorný, D., Alvarellos, J., Dones, L., & Levison, H. 2003, *AJ*, 126, 398.
- Nesvorný, D., Beauge, C. & Dones, L. 2004, *AJ*, 127, 1768.
- Nesvorný, D., Vokrouhlický, D. & Morbidelli, A. 2007, *AJ*, 133, 1962.
- Nesvorný, D., Vokrouhlický, D. & Deienno, R. 2014, *ApJ*, 784, 22.
- Nesvorný, D., Brož, M., Carruba, V., 2015. *Identification and Dynamical Properties of Asteroid Families. Asteroids IV*, Patrick Michel, Francesca E. DeMeo, and William F. Bottke (eds.), University of Arizona Press, Tucson, 895 pp. ISBN: 978-0-816-53213-1, 2015., p.297-321.
- Nesvorný, D. 2018, *ARAA*, 56, 137.
- Neveu, M. & Rhoden, A. 2019, *NatAs*, 3, 543.

- Nicholson, P., Cuk, M., Sheppard, S., Nesvorny, D. & Johnson, T. 2008. Irregular satellites of the giant planets. in: *The Solar System Beyond Neptune*, eds. M. Barucci, H. Boehnhardt, D. Cruikshank and A. Morbidelli, (The University of Arizona Press; Tucson) pp. 411-424.
- Nogueira, E., Brassier, R., & Gomes, R. 2011, *Icarus*, 214, 113.
- Parisi, M., Carraro, G., Maris, M. & Brunini, A. 2008, *AA*, 482, 657.
- Park, R., Folkner, W., Williams, J. & Boggs, D. 2021, *AJ*, 161, 105.
- Philpott, C., Hamilton, D. & Agnor, C. 2010, *Icarus*, 208, 824.
- Rufu, R. & Canup, R. 2017, *AJ*, 154, 208.
- Rufu, R. & Canup, R. 2022, *ApJ*, 928, 123.
- Salmon, J. & Canup, R. 2017, *ApJ*, 836, 109.
- Shankman, C., Gladman, B., Kaib, N., Kavelaars, J. & Petit, J. 2013, *ApJ*, 764, L2.
- Sharkey, B., Reddy, V., Kuhn, O., Sanchez, J. & Bottke, W. 2023, *PSJ*, 4, 223.
- Shen, Y. & Tremaine, S. 2008, *AJ*, 136, 2453.
- Sheppard, S. & Jewitt, D. 2003, *Nature*, 423, 261.
- Sheppard, S., Jewitt, D. & Kleyna, J. 2005, *AJ*, 129, 518.
- Sheppard, S., Jewitt, D. & Kleyna, J. 2006, *AJ*, 132, 171.
- Sheppard, S. & Trujillo, C. 2010, *ApJ*, 723, L233.
- Sheppard, S. & Trujillo, C. 2016, *AJ*, 152, 221.
- Sheppard, S., Tholen, D., & Trujillo, C. 2018, *RNAAS*, 7, 100.
- Sheppard, S., Tholen, D., Alexandersen, M. & Trujillo, C. 2023, *RNAAS*, 7, 100.
- Sheppard, S., Tholen, D., Trujillo, C., Lykawka, P. S., Brozovic, M. & Jacobson, R. 2024a, *MPEC* 2024-D112.
- Sheppard, S. et al. 2024b, *MPEC* 2024-D114.
- Sheppard, S., Tholen, D., Trujillo, C., Brozovic, M. & Jacobson, R. 2024c, *MPEC* 2024-D113.
- Showalter, M., de Pater, I., Lissauer, J. & French, R. 2019, *Nature*, 566, 350.
- Tamayo, D., Burns, J. & Hamilton, D. 2013, *Icarus*, 226, 655.
- Vokrouhlicky, D., Nesvorny, D. & Levison, H. 2008, *AJ*, 136, 1463.

Table 1. Fields Imaged Near Uranus and Neptune

UT Date	Tel	Center	RA and Dec	θ	Limit
yyyy/mm/dd			(hrs and degs)	($''$)	(m_r)
2021/09/03	Mag	NeptWest	23:30:43 -04:09:10	0.73	26.6
2021/09/03	Mag	NeptEast	23:32:39 -04:37:10	0.67	26.7
2021/09/07	Sub	NeptCenter	23:31:15 -04:19:43	0.83	27.2
2021/09/08	Sub	NeptCenter	23:31:09 -04:20:24	0.76	26.9
2021/09/08	Sub	UranCenter	02:48:01 +15:42:20	0.73	26.9
2021/10/06	Mag	S2002N5	23:27:52 -04:40:14	0.45	26.4
2021/10/06	Mag	S2021N1	23:30:23 -04:41:33	0.45	26.9
2021/10/29	Mag	UranSE	02:42:34 +15:08:46	0.9	26.3
2021/10/30	Mag	UranNE	02:42:32 +15:21:46	0.53	26.8
2021/10/30	Mag	UranSW	02:40:41 +15:08:03	0.62	26.7
2021/12/02	Mag	UranNW	02:35:32 +14:59:00	0.68	26.6
2021/12/06	Mag	UranSE	02:36:52 +14:36:19	0.84	26.5
2021/12/07	Mag	Uran2SW	02:34:44 +14:27:27	0.77	26.7
2021/12/07	Mag	S2002N5	23:24:46 -04:57:46	0.79	26.0
2022/10/15	Mag	S2002N5	23:37:09 -03:53:01	0.59	26.6
2022/10/16	Mag	S2002N5	23:37:15 -03:52:15	0.46	26.3
2022/11/16	VLT	S2021N1	23:36:25 -04:11:38	0.81	27.2
2023/11/03	Gem	S2021N1	23:45:28 -03:23:02	0.70	27.3
2023/11/04	Mag	21N1,02N5	23:45:01 -03:17:36	0.58	26.9
2023/11/04	Mag	UranCenter	03:15:07 +17:43:36	0.67	26.9
2023/12/06	Mag	S2023U1	03:09:44 +17:25:55	0.75	26.9
2023/12/13	Mag	S2023U1	03:08:57 +17:26:00	0.78	26.8

The telescopes (Tel) and wide-field instruments used were HyperSuprime-Cam on Subaru (Sub) and IMACS on Magellan (Mag). Recovery was done with IMACS as well as GMOS on Gemini North (Gem) and FORS2 on the VLT. Center is the planet observed: Neptune (Nept) or Uranus (Uran) along with the position of the detector relative to the planet or centered on a new moon observed. The Subaru observations always had the planet near the center of the detector. θ is the average seeing for the set of images and Limit is the limiting magnitude in the r-band where we would have found at least 75% of the satellites. Under the basic survey information for each night are the fields observed in J2000 coordinates for Right Ascension (RA hh:mm:ss) and Declination (Dec dd:mm:ss).

Table 2. New Absolute Astrometry And Residuals For Outer Satellites Of Neptune

Object	Site	Time UTC	α			δ			res. $\alpha\cos(\delta)$	res. δ
			hh	mm	ss	deg	mm	sec	arcsecond	arcsecond
Halimede	568	2021 09 07.45001	23	31	03.576	-04	12	28.66	0.127	-0.131
Halimede	568	2021 09 07.49866	23	31	03.277	-04	12	30.49	0.042	-0.072
Halimede	568	2021 09 08.45824	23	30	57.596	-04	13	07.75	-0.057	-0.010
Halimede	568	2021 09 08.48150	23	30	57.456	-04	13	08.50	-0.047	0.145
Halimede	568	2021 09 08.50087	23	30	57.330	-04	13	09.28	-0.182	0.118
Psamathe	568	2021 09 07.45442	23	33	18.749	-04	47	16.73	0.127	0.295
Psamathe	568	2021 09 07.52961	23	33	18.281	-04	47	20.08	0.047	-0.053
Psamathe	568	2021 09 08.45824	23	33	12.679	-04	47	57.15	0.132	0.001
Sao	568	2021 09 07.45885	23	32	07.372	-04	26	26.41	0.219	-0.011
Sao	568	2021 09 07.52961	23	32	06.925	-04	26	29.29	-0.041	-0.236
Sao	568	2021 09 08.45824	23	32	01.388	-04	27	03.84	-0.106	0.112
Sao	568	2021 09 08.48150	23	32	01.259	-04	27	04.88	0.085	-0.054
Sao	568	2021 09 08.50087	23	32	01.136	-04	27	05.44	0.009	0.114
Laomedeia	568	2021 09 07.45442	23	31	32.135	-04	12	23.72	-0.024	-0.306
Laomedeia	568	2021 09 07.49866	23	31	31.861	-04	12	25.30	0.061	-0.081
Laomedeia	568	2021 09 07.52961	23	31	31.667	-04	12	26.48	0.081	0.001
Laomedeia	568	2021 09 08.48150	23	31	25.759	-04	13	05.36	0.062	0.013
Laomedeia	568	2021 09 08.50087	23	31	25.640	-04	13	06.31	0.118	-0.146
Neso	568	2021 09 07.45001	23	33	11.178	-04	52	56.16	-0.091	0.181
Neso	568	2021 09 07.46327	23	33	11.091	-04	52	56.82	-0.165	0.055
Neso	568	2021 09 08.46987	23	33	04.979	-04	53	37.52	-0.190	0.023
Neso	568	2021 09 08.45824	23	33	05.047	-04	53	36.95	-0.128	-0.078
S/2002 N5	304	2021 09 03.16979	23	31	19.070	-04	17	09.73	0.404	0.557
S/2002 N5	304	2021 09 03.20208	23	31	18.880	-04	17	11.12	0.388	0.338
S/2002 N5	304	2021 09 03.24528	23	31	18.610	-04	17	12.87	0.132	0.153
S/2002 N5	568	2021 09 07.45885	23	30	54.198	-04	19	47.18	0.084	-0.245
S/2002 N5	568	2021 09 07.52961	23	30	53.766	-04	19	49.69	-0.081	-0.163
S/2002 N5	568	2021 09 08.45824	23	30	48.348	-04	20	23.69	-0.084	-0.078
S/2002 N5	568	2021 09 08.46597	23	30	48.301	-04	20	23.76	-0.097	0.135
S/2002 N5	568	2021 09 08.46987	23	30	48.265	-04	20	24.03	-0.288	0.009
S/2002 N5	568	2021 09 08.48924	23	30	48.161	-04	20	24.88	-0.114	-0.131

Table 2 continued on next page

Table 2 (*continued*)

Object	Site	Time	α	δ	res. $\alpha\cos(\delta)$	res. δ
		UTC	hh mm ss	deg mm sec	arcsecond	arcsecond
S/2002 N5	568	2021 09 08.49311	23 30 48.143	-04 20 25.12	-0.038	-0.229
S/2002 N5	568	2021 09 08.50087	23 30 48.107	-04 20 25.19	0.116	-0.014
S/2002 N5	304	2021 10 06.05016	23 28 09.955	-04 36 45.38	0.064	-0.084
S/2002 N5	304	2021 10 06.05974	23 28 09.899	-04 36 45.73	0.006	-0.120
S/2002 N5	304	2021 12 07.05600	23 25 26.695	-04 52 02.60	-0.341	-0.344
S/2002 N5	304	2022 10 15.06092	23 37 02.582	-03 47 17.28	0.011	-0.102
S/2002 N5	304	2022 10 15.13403	23 37 02.195	-03 47 19.68	-0.090	-0.050
S/2002 N5	304	2022 10 16.06909	23 36 57.474	-03 47 50.71	-0.040	0.055
S/2002 N5	304	2022 10 16.08325	23 36 57.398	-03 47 51.34	-0.088	-0.106
S/2002 N5	304	2022 10 16.09739	23 36 57.341	-03 47 51.55	0.147	0.151
S/2002 N5	304	2023 11 04.04097	23 44 26.210	-03 11 35.83	-0.306	0.153
S/2002 N5	304	2023 11 04.12662	23 44 25.922	-03 11 38.18	0.402	-0.132
S/2021 N1	568	2021 09 07.45001	23 33 34.149	-04 19 20.31	0.117	-0.170
S/2021 N1	568	2021 09 07.48980	23 33 33.890	-04 19 21.93	-0.134	-0.175
S/2021 N1	568	2021 09 07.52961	23 33 33.668	-04 19 23.51	0.167	-0.140
S/2021 N1	568	2021 09 08.45824	23 33 28.114	-04 20 01.13	0.020	-0.009
S/2021 N1	568	2021 09 08.50087	23 33 27.866	-04 20 02.84	0.204	0.014
S/2021 N1	304	2021 10 06.09365	23 30 44.708	-04 38 09.62	-0.020	0.129
S/2021 N1	304	2021 10 06.10324	23 30 44.654	-04 38 09.79	-0.017	0.307
S/2021 N1	304	2021 10 06.13223	23 30 44.428	-04 38 11.08	-0.947	0.068
S/2021 N1	309	2022 11 16.02415	23 36 28.290	-04 11 34.49	-0.047	-0.040
S/2021 N1	309	2022 11 16.12292	23 36 28.057	-04 11 35.74	0.019	0.027
S/2021 N1	568	2023 11 03.20694	23 45 28.539	-03 23 03.60	-0.075	0.102
S/2021 N1	568	2023 11 03.27194	23 45 28.281	-03 23 05.05	-0.028	0.216
S/2021 N1	304	2023 11 04.04097	23 45 25.308	-03 23 23.46	0.039	-0.167
S/2021 N1	304	2023 11 04.12639	23 45 24.975	-03 23 25.46	0.091	-0.162

NOTE—Residuals for absolute astrometry in Right Ascension (α) and Declination (δ). Results use the Neptune satellites nep104 orbit solutions from the JPL *Horizons* On-Line Solar System Data Service (Acton 1996) and from NASA's Navigation and Ancillary Information Facility (Giorgini et al. 1996) (ssd.jpl.nasa.gov/sats). Site codes are 568 for Mauna Kea in Hawaii, 304 for Magellan at Las Campanas in Chile and 309 for the Very Large Telescope in Chile.

Table 3. New Absolute Astrometry and Residuals For The Outer Satellites Of Uranus

Object	Site	Time UTC	α	δ	res. $\alpha\cos(\delta)$	res. δ
			hh mm ss	deg mm sec	arcsecond	arcsecond
Caliban	568	2021 09 08.50737	02 47 37.867	+15 37 34.32	-0.048	-0.111
Caliban	568	2021 09 08.52656	02 47 37.794	+15 37 33.88	-0.058	-0.194
Caliban	568	2021 09 08.54960	02 47 37.705	+15 37 33.37	-0.086	-0.272
Caliban	304	2021 10 30.21467	02 41 24.923	+15 08 11.58	-0.114	0.031
Caliban	304	2023 11 04.14634	03 15 36.150	+17 47 08.14	-0.107	-0.180
Caliban	304	2023 11 04.18390	03 15 35.783	+17 47 06.93	0.073	-0.123
Caliban	304	2023 11 04.23291	03 15 35.280	+17 47 05.28	-0.045	-0.108
Sycorax	568	2021 09 08.50737	02 47 27.293	+15 36 26.14	0.009	0.047
Sycorax	568	2021 09 08.52656	02 47 27.214	+15 36 25.70	-0.033	-0.084
Sycorax	568	2021 09 08.54960	02 47 27.121	+15 36 25.40	-0.053	-0.009
Sycorax	304	2021 10 30.17326	02 41 03.834	+15 08 44.64	-0.061	0.004
Sycorax	304	2021 10 30.21467	02 41 03.426	+15 08 42.96	-0.068	0.055
Sycorax	304	2021 10 30.25226	02 41 03.057	+15 08 41.33	-0.055	0.003
Prospero	304	2021 10 30.23342	02 40 02.339	+15 16 54.72	0.279	-0.237
Prospero	304	2021 10 30.24475	02 40 02.214	+15 16 54.20	0.072	-0.266
Prospero	304	2021 10 30.25605	02 40 02.105	+15 16 53.79	0.100	-0.185
Prospero	304	2023 11 04.14634	03 15 46.483	+17 38 52.11	-0.112	0.190
Prospero	304	2023 11 04.18013	03 15 46.143	+17 38 50.79	-0.017	0.245
Prospero	304	2023 12 06.11627	03 10 26.561	+17 17 13.55	-0.063	0.075
Prospero	304	2023 12 06.18583	03 10 25.915	+17 17 11.01	0.016	0.140
Setebos	568	2021 09 08.51120	02 48 27.552	+15 53 29.32	-0.150	0.112
Setebos	568	2021 09 08.52656	02 48 27.502	+15 53 29.05	-0.052	0.059
Setebos	568	2021 09 08.54576	02 48 27.424	+15 53 28.89	-0.160	0.172
Setebos	304	2021 10 30.26006	02 42 13.952	+15 26 28.06	-0.049	0.191
Setebos	304	2021 10 30.33414	02 42 13.233	+15 26 24.89	-0.058	0.185
Stephano	568	2021 09 08.50737	02 47 36.365	+15 42 04.72	0.009	-0.050
Stephano	568	2021 09 08.52656	02 47 36.287	+15 42 04.26	0.016	-0.108
Stephano	568	2021 09 08.54960	02 47 36.195	+15 42 03.72	0.054	-0.162
Stephano	304	2021 10 30.17326	02 41 06.654	+15 09 47.98	-0.130	0.251
Stephano	304	2021 10 30.21467	02 41 06.238	+15 09 45.94	-0.179	0.181
Stephano	304	2021 10 30.25226	02 41 05.866	+15 09 44.10	-0.141	0.136

Table 3 continued on next page

Table 3 (*continued*)

Object	Site	Time	α	δ	res. $\alpha\cos(\delta)$	res. δ
		UTC	hh mm ss	deg mm sec	arcsecond	arcsecond
Trinculo	568	2021 09 08.50737	02 47 37.865	+15 41 40.78	-0.071	0.005
Trinculo	568	2021 09 08.52656	02 47 37.785	+15 41 40.56	-0.060	0.168
Trinculo	568	2021 09 08.54960	02 47 37.694	+15 41 39.93	0.032	0.001
Trinculo	304	2021 10 30.17326	02 41 03.668	+15 10 30.31	-0.068	0.226
Trinculo	304	2021 10 30.21467	02 41 03.232	+15 10 28.30	-0.383	0.123
Trinculo	304	2021 10 30.25226	02 41 02.882	+15 10 26.48	0.016	0.040
Francisco	568	2021 09 08.50737	02 48 17.928	+15 45 49.77	0.179	-0.356
Francisco	568	2021 09 08.52656	02 48 17.861	+15 45 49.70	0.406	-0.140
Francisco	568	2021 09 08.54960	02 48 17.757	+15 45 49.18	0.329	-0.313
Francisco	304	2023 11 04.14258	03 15 28.107	+17 44 27.39	-0.005	-0.092
Francisco	304	2023 11 04.14634	03 15 28.068	+17 44 27.26	-0.006	-0.090
Francisco	304	2023 12 06.06707	03 10 01.555	+17 25 24.57	-0.357	0.257
Francisco	304	2023 12 06.07125	03 10 01.518	+17 25 24.44	-0.306	0.267
Margaret	568	2021 09 08.50737	02 47 28.368	+15 19 24.09	-0.322	-0.097
Margaret	568	2021 09 08.52656	02 47 28.303	+15 19 23.76	-0.155	-0.096
Margaret	568	2021 09 08.54960	02 47 28.213	+15 19 23.47	-0.130	0.015
Margaret	304	2021 12 07.10835	02 35 15.415	+14 25 09.89	0.126	0.118
Margaret	304	2021 12 07.12760	02 35 15.266	+14 25 09.30	0.139	0.155
Ferdinand	568	2021 09 08.50737	02 49 12.416	+15 53 39.87	-0.044	0.037
Ferdinand	568	2021 09 08.52656	02 49 12.341	+15 53 39.61	-0.030	0.109
Ferdinand	568	2021 09 08.54960	02 49 12.245	+15 53 39.05	-0.097	-0.049
Ferdinand	304	2021 10 30.26006	02 42 43.789	+15 24 03.30	-0.141	0.010
Ferdinand	304	2021 10 30.29707	02 42 43.438	+15 24 01.76	0.149	0.152
Ferdinand	304	2021 10 30.33414	02 42 43.059	+15 23 59.86	0.015	-0.059
S/2023 U1	568	2021 09 08.50737	02 47 38.560	+15 44 01.37	0.013	0.196
S/2023 U1	568	2021 09 08.53040	02 47 38.453	+15 44 00.74	-0.292	-0.123
S/2023 U1	304	2021 12 02.12835	02 36 24.703	+14 56 07.10	0.242	-0.124
S/2023 U1	304	2021 12 02.20226	02 36 24.096	+14 56 04.33	0.159	-0.296
S/2023 U1	304	2023 11 04.14258	03 15 15.924	+17 49 32.61	-0.203	0.257
S/2023 U1	304	2023 11 04.19892	03 15 15.383	+17 49 30.43	0.014	0.111
S/2023 U1	304	2023 11 04.24063	03 15 14.992	+17 49 28.77	0.322	-0.033
S/2023 U1	304	2023 12 06.06707	03 10 09.059	+17 29 53.08	-0.311	0.050
S/2023 U1	304	2023 12 06.18594	03 10 08.016	+17 29 48.92	0.047	0.015

Table 3 continued on next page

Table 3 (*continued*)

Object	Site	Time	α	δ	res. $\alpha\cos(\delta)$	res. δ
		UTC	hh mm ss	deg mm sec	arcsecond	arcsecond
S/2023 U1	304	2023 12 13.09425	03 09 09.764	+17 25 58.03	-0.174	-0.054
S/2023 U1	304	2023 12 13.20694	03 09 08.857	+17 25 54.51	0.085	0.060

NOTE—Residuals for absolute astrometry in Right Ascension (α) and Declination (δ). Results use the Uranus satellites ura117 orbit solutions from the JPL *Horizons* On-Line Solar System Data Service (Acton 1996) and from NASAs Navigation and Ancillary Information Facility (Giorgini et al. 1996) (ssd.jpl.nasa.gov/sats). Site codes are 568 for Subaru on Mauna Kea in Hawaii and 304 for Magellan at Las Campanas in Chile.

Table 4. New Satellites of Uranus and Neptune

Name	a (AU)	e	i (deg)	Ω (deg)	ω (deg)	M (deg)	P (yrs)	Dia (km)	m_r (mag)	H (mag)
S/2023 U1	0.0533	0.187	141.89	265.84	142.16	24.08	1.86	7	26.6	13.7
S/2002 N5	0.1562	0.548	42.133	274.15	62.73	105.52	8.60	23	25.9	11.2
S/2021 N1	0.338	0.441	134.5	264.1	100.8	86.4	27.4	14	26.9	12.1

Quantities are the current new satellite orbits from the Minor Planet Electronic Circulars (MPECs) on the discovery of the new satellites published by the Minor Planet Center (Sheppard et al. 2024a,2024b,2024c). Columns are the semi-major axis (a), eccentricity (e), inclination (i), longitude of the ascending node (Ω), argument of perihelion (ω), and Mean Anomaly (M) for Epoch 2024 Mar 31.0 with significant digits showing the size of uncertainty. Diameter (Dia) estimates assume a moderate albedo of 0.10. The r-band magnitude (m_r) is the opposition magnitude.

Table 5. Mean Osculating Orbital Elements For Outer Satellites Of Uranus

Satellite	Osc. a (km)	Osc. e	Osc. i (deg)	Osc. P (d)
Francisco	4275700 ⁺⁷⁰⁰ ₋₇₀₀	0.14 ^{+0.05} _{-0.05}	147 ⁺² ₋₁	267 ⁺¹ ₋₁
Caliban	7167000 ⁺⁵⁴⁰⁰ ₋₅₄₀₀	0.20 ^{+0.12} _{-0.13}	141 ⁺³ ₋₂	580 ⁺¹ ₋₁
Stephano	7951400 ⁺⁸⁶⁰⁰ ₋₈₀₀₀	0.23 ^{+0.11} _{-0.11}	144 ⁺³ ₋₃	677 ⁺¹ ₋₁
S/2023 U1	7976600 ⁺⁸⁶⁰⁰ ₋₈₆₀₀	0.25 ^{+0.11} _{-0.11}	144 ⁺³ ₋₃	681 ⁺¹ ₋₁
Trinculo	8502600 ⁺¹²²⁰⁰ ₋₁₀₆₀₀	0.22 ^{+0.02} _{-0.02}	167 ⁺¹ ₋₁	749 ⁺² ₋₁
Sycorax	12193200 ⁺⁶⁵²⁰⁰ ₋₅₁₉₀₀	0.52 ^{+0.08} _{-0.08}	157 ⁺⁶ ₋₆	1286 ⁺¹⁰ ₋₈
Margaret	14425000 ⁺¹¹³⁵⁰⁰ ₋₁₀₆₅₀₀	0.64 ^{+0.25} _{-0.23}	61 ⁺⁸ ₋₁₅	1655 ⁺²⁰ ₋₁₈
Prospero	16221000 ⁺¹⁸³⁶⁰⁰ ₋₁₄₆₂₀₀	0.44 ^{+0.14} _{-0.13}	149 ⁺⁶ ₋₆	1974 ⁺³⁴ ₋₂₇
Setebos	17519800 ⁺²⁷⁸³⁰⁰ ₋₂₂₁₃₀₀	0.58 ^{+0.13} _{-0.12}	154 ⁺⁸ ₋₈	2215 ⁺⁵³ ₋₄₂
Ferdinand	20421400 ⁺⁴⁵⁵⁹⁰⁰ ₋₃₃₈₅₀₀	0.40 ^{+0.09} _{-0.09}	169 ⁺³ ₋₂	2788 ⁺⁹⁴ ₋₆₉

NOTE—Osculating orbital elements, a , e , and i , represent the mean and the extreme osculating values obtained from 10,000 years of integrated orbits. The elements were generated with respect to the ecliptic pole RA=270.00 and Dec=66.56 degrees.

Table 6. Mean Osculating Orbital Elements For Outer satellites Of Neptune

Satellite	Osc. a (km)	Osc. e	Osc. i (deg)	Osc. P (d)
Halimede	16590500 ⁺⁴²⁰⁰⁰ ₋₃₆₇₀₀	0.52 ^{+0.38} _{-0.33}	120 ⁺²⁵ ₋₉	1879 ⁺⁷ ₋₆
Sao	22239900 ⁺¹²⁸²⁰⁰ ₋₁₁₆₉₀₀	0.30 ^{+0.33} _{-0.23}	50 ⁺⁵ ₋₁₁	2917 ⁺²⁵ ₋₂₃
S/2002 N5	23414700 ⁺¹⁷²⁸⁰⁰ ₋₁₅₁₇₀₀	0.43 ^{+0.24} _{-0.21}	46 ⁺⁸ ₋₁₀	3151 ⁺³⁵ ₋₃₁
Laomedeia	23499900 ⁺¹⁸⁶⁰⁰⁰ ₋₁₅₂₀₀₀	0.42 ^{+0.14} _{-0.13}	37 ⁺⁷ ₋₇	3168 ⁺³⁸ ₋₃₁
Psamathe	47646600 ⁺²⁵²²⁴⁰⁰ ₋₁₉₈₃₄₀₀	0.41 ^{+0.47} _{-0.34}	128 ⁺²⁰ ₋₁₁	9149 ⁺⁷³⁵ ₋₅₆₆
Neso	49897800 ⁺²⁹¹²⁹⁰⁰ ₋₂₂₄₂₅₀₀	0.46 ^{+0.42} _{-0.32}	128 ⁺¹⁷ ₋₁₁	9805 ⁺⁸⁷⁰ ₋₆₅₅
S/2021 N1	50700200 ⁺²⁹⁷⁷²⁰⁰ ₋₂₂₅₃₁₀₀	0.50 ^{+0.21} _{-0.18}	135 ⁺⁷ ₋₇	10043 ⁺⁷¹³ ₋₆₆₄

NOTE—Osculating orbital elements, a , e , and i , represent the mean and the extreme osculating values obtained from 10,000 years of integrated orbits. The elements were generated with respect to the ecliptic pole, RA=270.00 and Dec=66.56 degs.

Table 7. Dispersion Velocity Between Satellite Group Members

Objects	δV (<i>m/s</i>)	δV_{min} (<i>m/s</i>)
Uranian Caliban Group		
Caliban-Stephano	257 ± 47	210
Caliban-S/2023U1	267 ± 51	216
Stephano-S/2023U1	66 ± 45	21
Neptunian Sao Group		
Sao-Laomedea	200 ± 62	138
Sao-S/2002N5	143 ± 76	67
Laomedea-S/2002N5	145 ± 47	98
Neptunian Neso Group		
Psamathe-Neso	120 ± 79	41
Psamathe-S/2021N1	123 ± 47	76
Neso-S/2021N1	107 ± 46	61

NOTE— δV is the dispersion velocity between members in m/s while δV_{min} is the minimal dispersion velocity. The dispersion velocity and its range were calculated over 30,000 years of orbital simulation with a data step of 100 days.

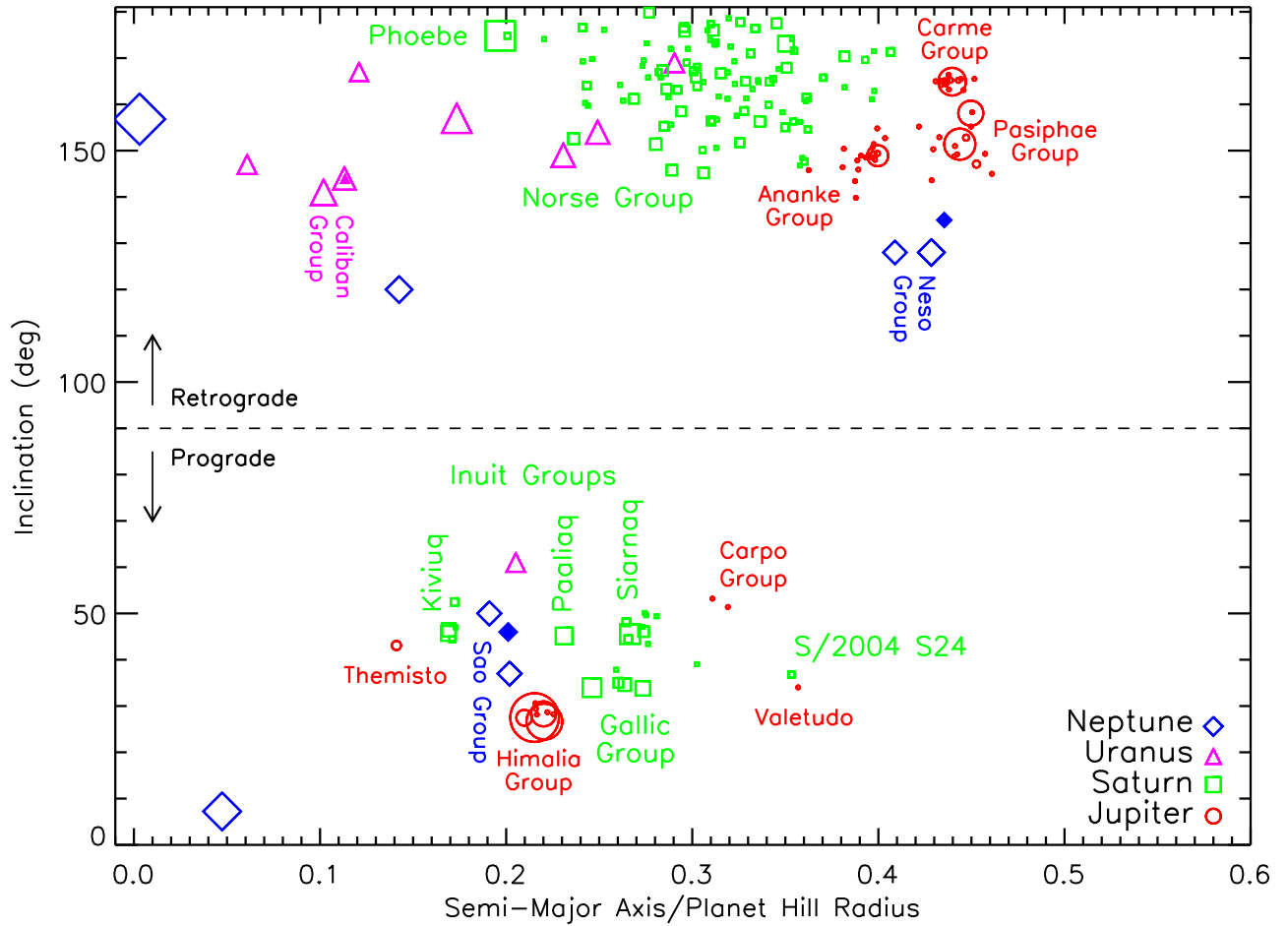


Figure 1. The known outer satellites of the giant planets where Neptunians are blue diamonds, Uranians magenta triangles, Saturnians green squares and Jovians red circles. Symbol size is proportional to the Log of the diameter of the satellite. Semi-major axis and inclination are the mean osculating orbital elements from this work for Uranus and Neptune, from Jacobson et al. (2022) for Saturn and Brozovic & Jacobson (2017) for Jupiter with updates from new discoveries at Jupiter and Saturn reported in Sheppard et al. (2018, 2023) and Ashton et al. (2020, 2021, 2022) shown at ssd.jpl.nasa.gov/sats/elem. The newly discovered Uranus and Neptune satellites reported here are shown as filled solid symbols while already known satellites are shown by open symbols. As seen here, all known outer satellites have semi-major axes less than 0.5 Hill radii. Dynamical families are identified by the largest member. The new Uranian satellite S/2023 U1 has a similar orbit as Caliban and Stephano, making this the first group of three or more satellites known at Uranus. The new Neptunian S/2021 N1 has a similar distant retrograde orbit as Neso and Psamathe, while the new S/2002 N5 has a similar prograde orbit as Sao and Laomedea, making both these the first known groups of three or more satellites at Neptune.

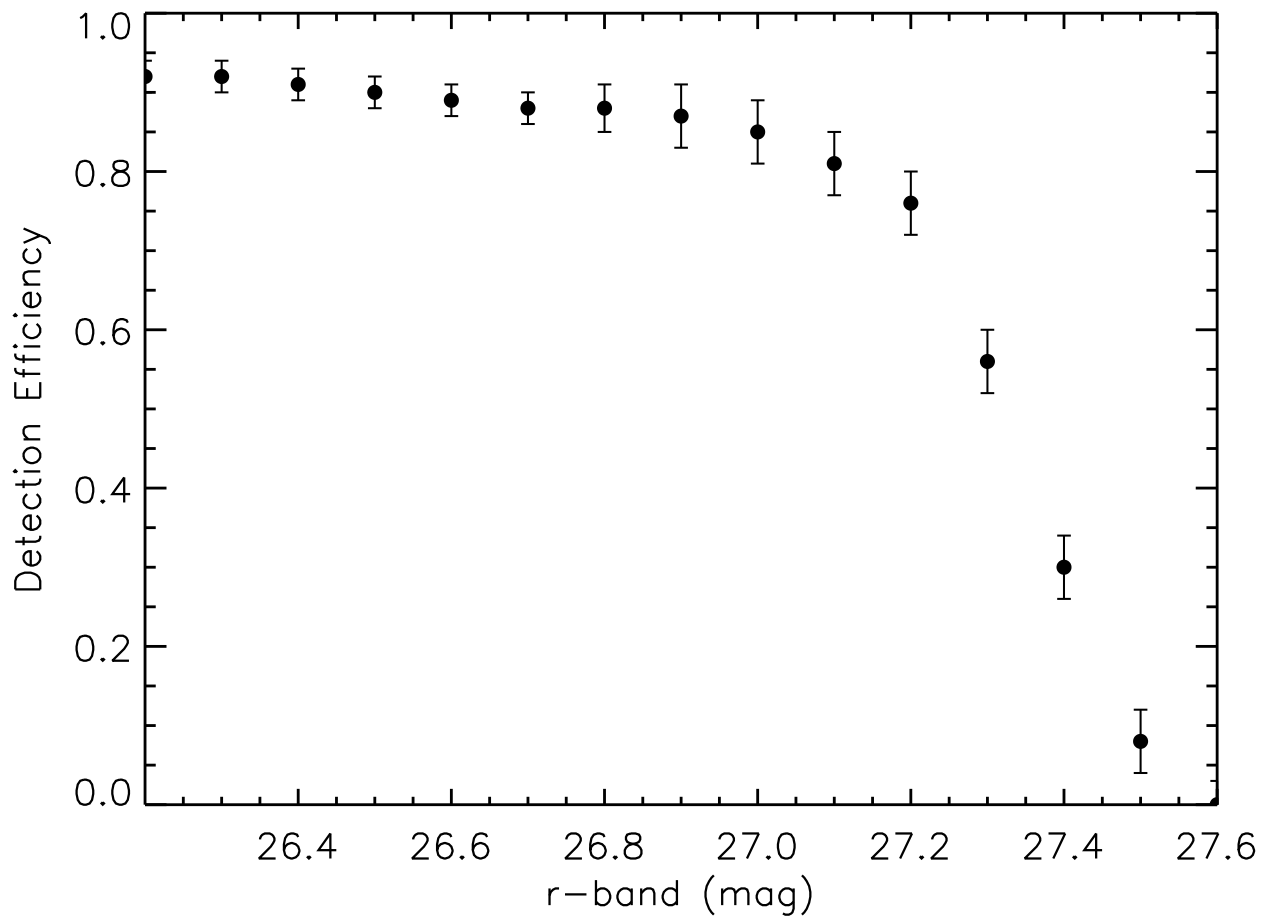


Figure 2. The efficiency of searching the Subaru September 7, 2021 data for Neptune satellites. We would expect to find over 75 percent of satellites within the field of view of HSC at 27.2 magnitudes in the r-band, which we take as the limiting magnitude of this one night. Table 1 shows all the detection efficiencies for the various nights of observations at Uranus and Neptune.

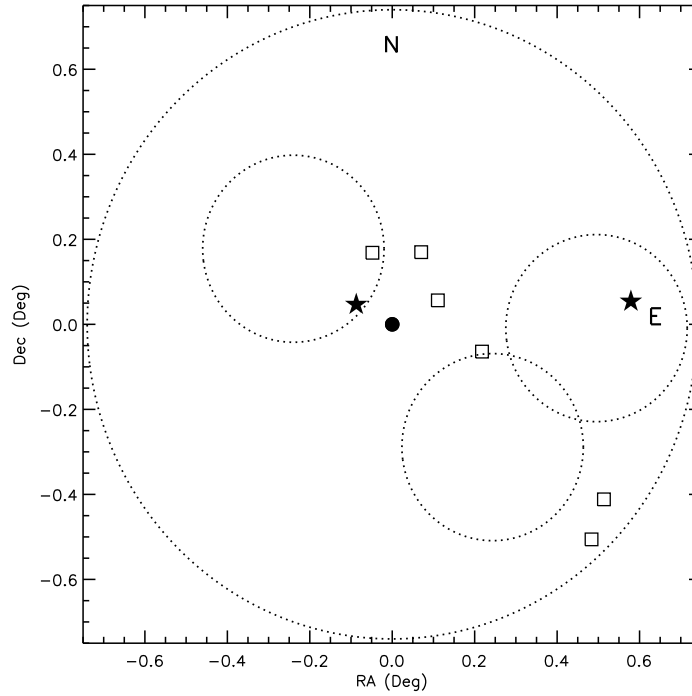


Figure 3. Area searched around Neptune in 2021. Known outer Neptune satellite positions are shown as open square symbols for September 7, 2021. Neptune is at the center of the field shown by the filled circle. The large dotted circle is the field of view of HyperSuprime-Cam on Subaru. The smaller dotted circles are the fields imaged with IMACS on Magellan that went to a depth beyond 26.5 mags taken on September 3 and October 6 in 2021 (see Table 1). All known outer satellites of Neptune were detected. The newly discovered Neptune satellites S/2021 N1 (near far East edge) and S/2002 N5 (near Neptune) are shown by filled stars.

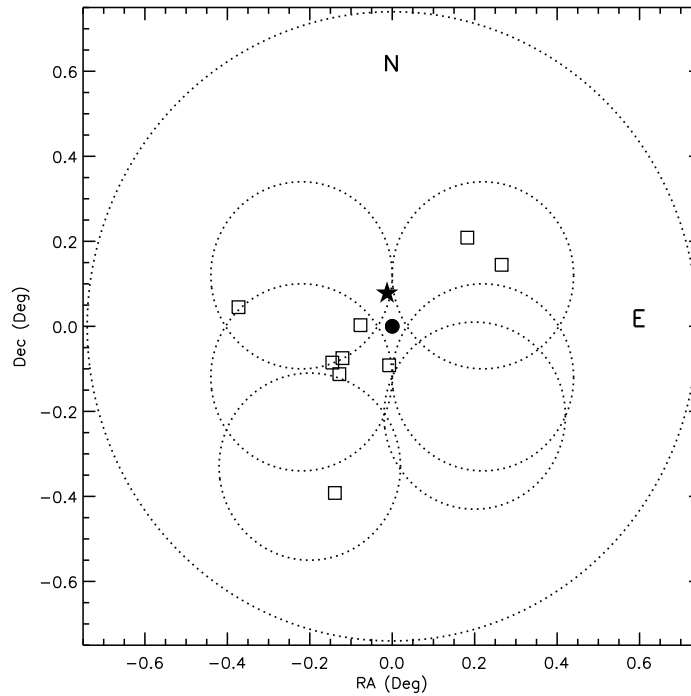


Figure 4. Area searched around Uranus in 2021. Known outer Uranus satellite positions are shown as open square symbols for December 2, 2021. Uranus is at the center of the field shown by the filled circle. The large dotted circle is the field of view of HyperSuprime-Cam on Subaru and the smaller dotted circles are the fields imaged with IMACS on Magellan (see Table 1). The Southeast quadrant has two, mostly overlapping, fields since this area was re-imaged in December 2021 with IMACS as the October 2021 observations had poor seeing. All known outer satellites of Uranus were detected. The newly discovered Uranus satellite S/2023 U1 is shown by a filled star.

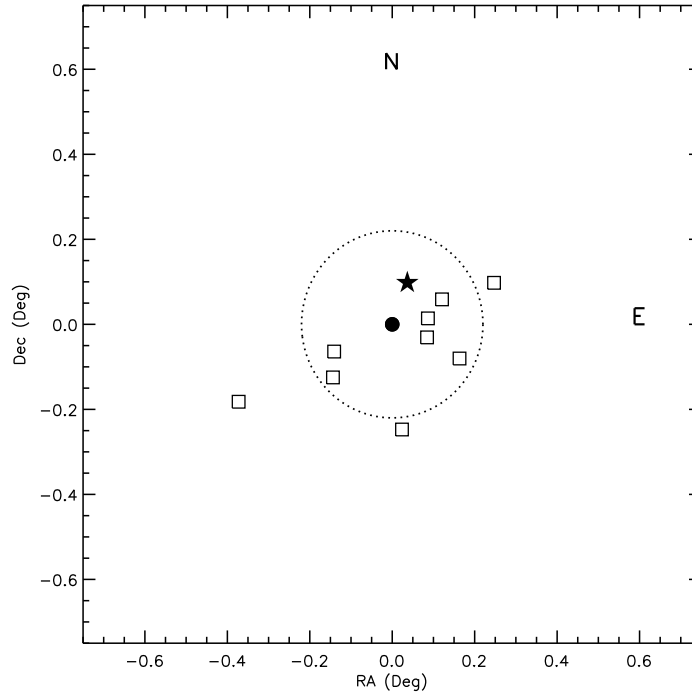


Figure 5. Area searched around Uranus in 2023. Known outer Uranus satellite positions are shown as open square symbols for November 4, 2023. The dotted circle is the field-of-view imaged with IMACS on Magellan on three different nights in November and December 2023 with Uranus placed at the center of the field (see Table 1). The newly discovered Uranus satellite S/2023 U1 is shown by a filled star. The Magellan observations of 2023 had 6 of the 9 known outer satellites of Uranus easily detected with only the most distant satellites outside the field of view undetected.

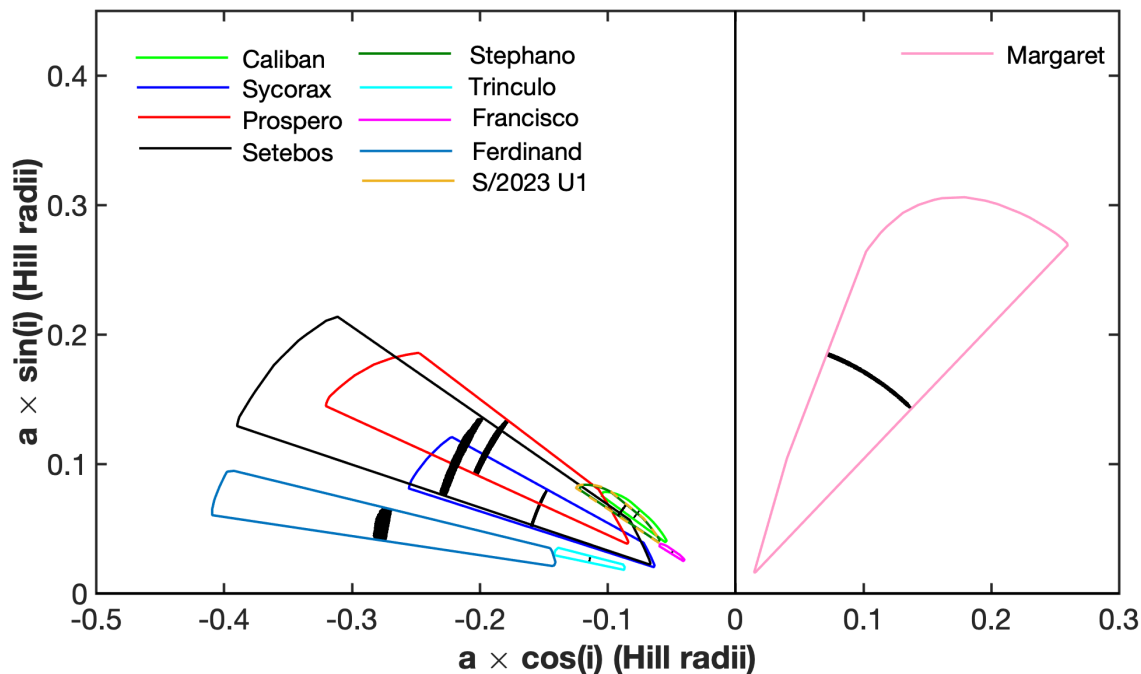


Figure 6. Orbital phase space for the irregular satellites of Uranus. Black dots show osculating semi-major axis multiplied by sines and cosines of the osculating inclination, while the colored outlines show the pericenter-to-apocenter variation, $2ae$, for the duration of 10000 years. The reference plane for inclinations is the ecliptic. The Hill radius for Uranus is 0.47 au. The newly discovered satellite S/2023 U1 (in orange) completely overlaps in phase space with Stephano.

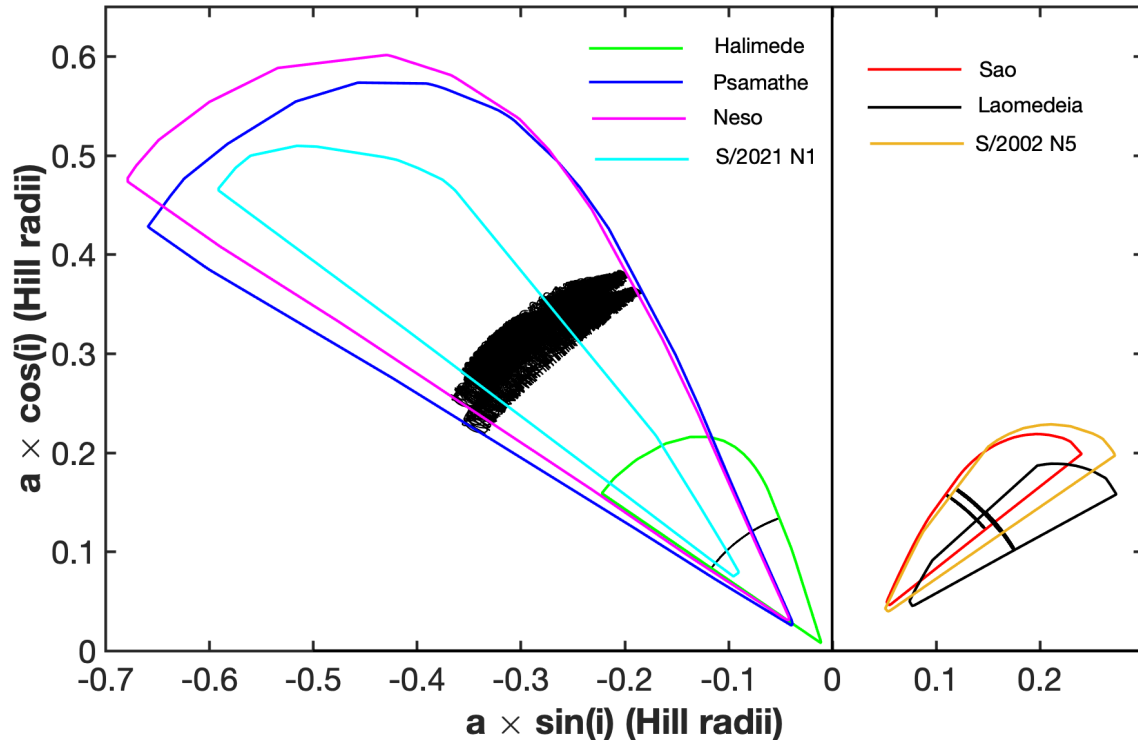


Figure 7. Orbital phase space for the irregular satellites of Neptune. Black dots show osculating semi-major axis multiplied by sines and cosines of the osculating inclination, while the colored outlines show the pericenter-to-apocenter variation, $2ae$, for the duration of 10,000 years. The reference plane for inclinations is the ecliptic. The Hill radius for Neptune is 0.77 au.

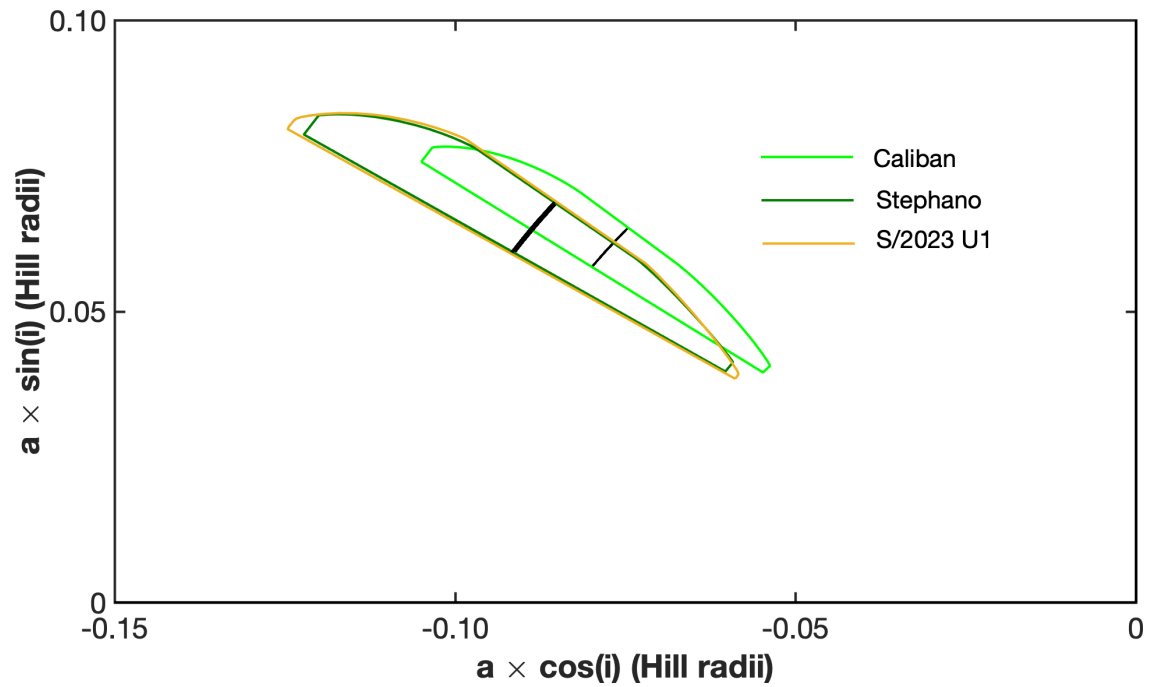


Figure 8. Caliban group of satellites. The newly discovered satellite S/2023 U1 (in orange) completely overlaps in phase space with Stephano. We investigated how close they can approach to each other within 30,000 years of orbit integration: Stephano and S/2023 U1 could have about a 22,000 km encounter around 5176 AD.

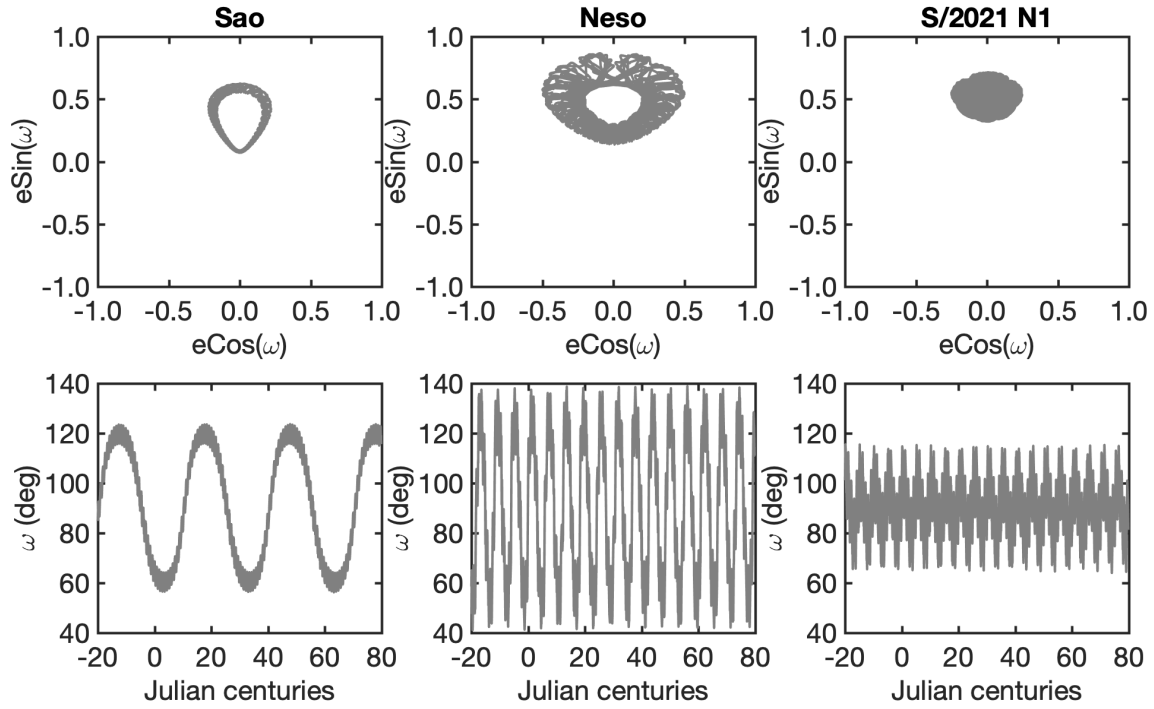


Figure 9. Representation of the Kozai–Lidov dynamics for Neptune satellites Sao, Neso, and new S/2021 N1. The top panels show osculating $(e\cos(\omega), e\sin(\omega))$, while the bottom panels show the osculating argument of pericenter (ω) for 10,000 years of orbit integration. The argument of pericenter librates around 90 deg. The reference plane for inclination is the orbital plane of Neptune around the Sun with the mean pole of RA 273.46 and Dec 67.71 degrees. The mean pole is estimated from de441 planetary ephemeris.

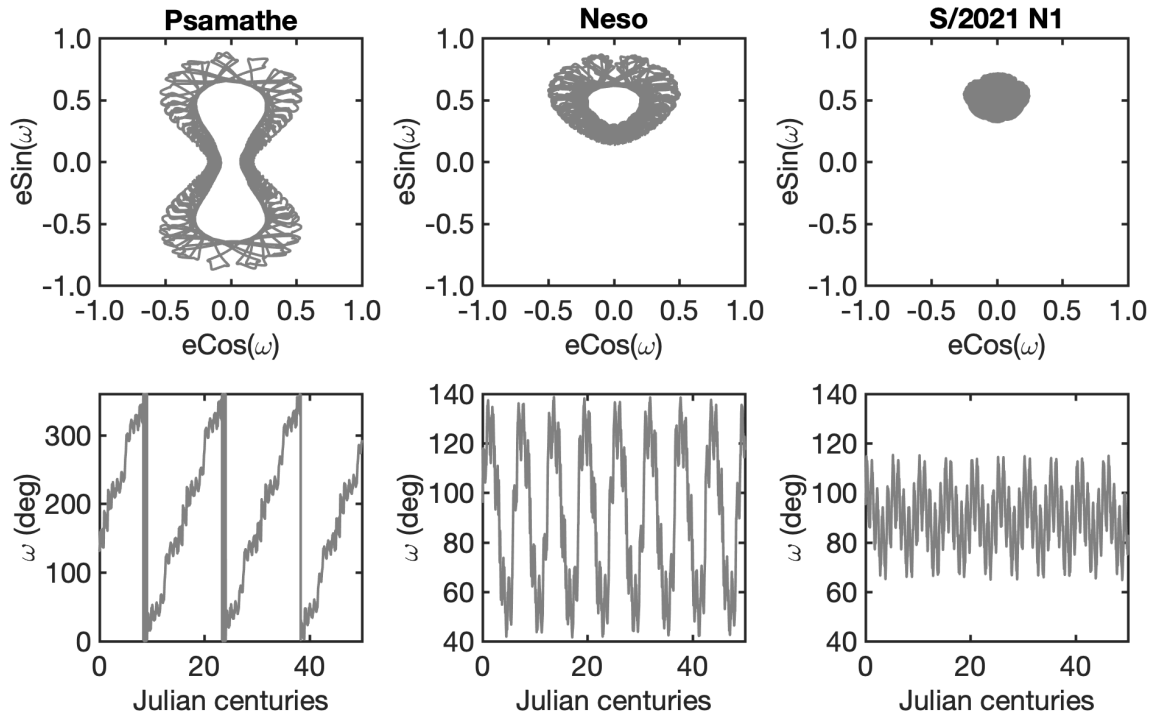


Figure 10. Same as Figure 9 but for the Neso group of Neptune satellites. Neso and new satellite S/2021 N1 are in Kozai-Lidov resonance with their argument of pericenter oscillating around 90 deg, but Psamathe is not in this resonance.

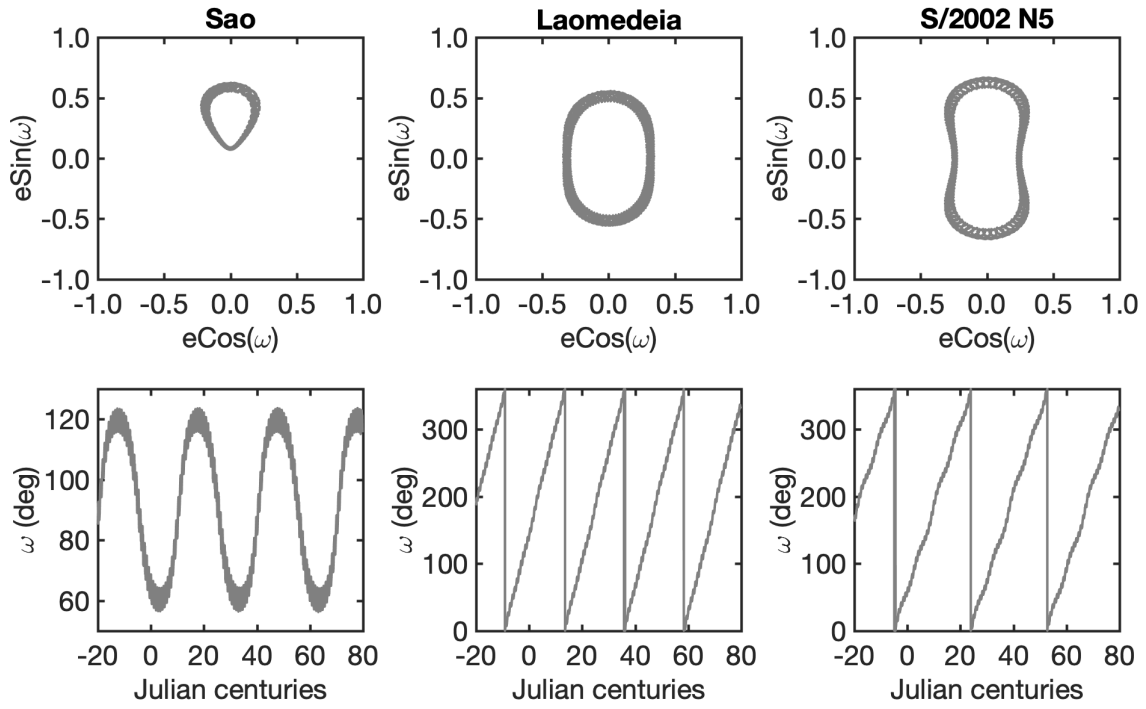


Figure 11. Same as Figure 9 but for the Sao group of Neptune satellites. Sao is in the Kozai-Lidov resonance with its argument of pericenter oscillating around 90 deg, but other dynamical group members Laomedea and S/2002 N5 are not in this resonance.

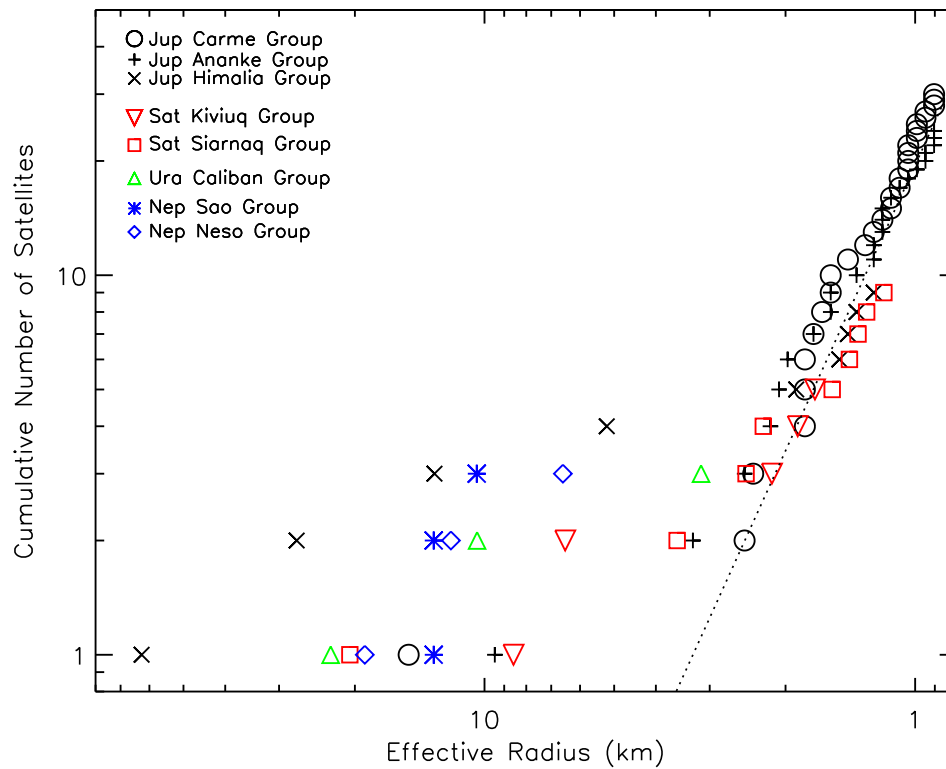


Figure 12. The cumulative size distribution for the various well-determined outer irregular satellite dynamical families around the giant planets. Most dynamical satellite families have a few large to medium members and many more smaller members. A typical steep collisional size distribution is apparent for satellites smaller than about 5 km in size, whereas larger satellites have a much shallower distribution. The dotted line shows the canonical Dohnanyi (1972) asteroid collisional power law of $q = -2.5$, which fits the smaller satellites of less than 5 km well. This indicates the smallest known satellites are consistent with a collisional origin.